Molecular Biology of the Cell
Vol. 12, 1481–1498, May 2001

Quantitative ER ↔ Golgi Transport Kinetics and Protein Separation upon Golgi Exit Revealed by Vesicular Integral Membrane Protein 36 Dynamics in Live Cells[V]

Thorsten Dahm,*†§# Jamie White,*†‖¶# Stephan Grill,*† Joachim Füllekrug,†‡ and Ernst H.K. Stelzer†‡

*Light Microscopy Group and †Cell Biology and Biophysics Programme, European Molecular Biology Laboratory, D-69117 Heidelberg, Germany; ‡Max Planck Institute for Molecular Cell Biology and Genetics, D-01307 Dresden, Germany

Submitted July 31, 2000; Revised January 10, 2001; Accepted February 22, 2001
Monitoring Editor: Jennifer Lippincott-Schwartz

To quantitatively investigate the trafficking of the transmembrane lectin VIP36 and its relation to cargo-containing transport carriers (TCs), we analyzed a C-terminal fluorescent-protein (FP) fusion, VIP36-SP-FP. When expressed at moderate levels, VIP36-SP-FP localized to the endoplasmic reticulum, Golgi apparatus, and intermediate transport structures, and colocalized with epitope-tagged VIP36. Temperature shift and pharmacological experiments indicated VIP36-SP-FP recycled in the early secretory pathway, exhibiting trafficking representative of a class of transmembrane cargo receptors, including the closely related lectin ERGIC53. VIP36-SP-FP trafficking structures comprised tubules and globular elements, which translocated in a saltatory manner. Simultaneous visualization of anterograde secretory cargo and VIP36-SP-FP indicated that the globular structures were pre-Golgi carriers, and that VIP36-SP-FP segregated from cargo within the Golgi and was not included in post-Golgi TCs. Organelle-specific bleach experiments directly measured the exchange of VIP36-SP-FP between the Golgi and endoplasmic reticulum (ER). Fitting a two-compartment model to the recovery data predicted first order rate constants of 1.22 ± 0.44%/min for ER → Golgi, and 7.68 ± 1.94%/min for Golgi → ER transport, revealing a half-time of 113 ± 70 min for leaving the ER and 1.67 ± 0.45 min for leaving the Golgi, and accounting for the measured steady-state distribution of VIP36-SP-FP (13% Golgi/87% ER). Perturbing transport with AlF_4^- treatment altered VIP36-SP-GFP distribution and changed the rate constants. The parameters of the model suggest that relatively small differences in the first order rate constants, perhaps manifested in subtle differences in the tendency to enter distinct TCs, result in large differences in the steady-state localization of secretory components.

INTRODUCTION

The integral membrane lectin VIP36 belongs to a family of lectins, conserved from yeast to mammals, trafficking in the secretory pathway (Fiedler and Simons, 1994). The closely related lectin ERGIC-53 acts as a cargo receptor, facilitating endoplasmic reticulum (ER) to Golgi transport of certain glycoproteins (Nichols *et al.*, 1998; Vollenweider *et al.*, 1998; Appenzeller *et al.*, 1999), but a function for VIP36 in intracellular transport is yet to be demonstrated. VIP36 was originally identified as a component of apical post-Golgi vesicles in virally infected, polarized Madin-Darby canine kidney cells (Wandinger-Ness *et al.*, 1990; Fiedler *et al.*, 1994). Localization of overexpressed VIP36 to the plasma membrane, endosomes, and Golgi structures, together with evidence for lectin activity (Fiedler and Simons, 1996; Hara-Kuge *et al.*, 1999) lead to the hypothesis that it functioned to segregate apical cargo into distinct vesicles within the *trans*-Golgi network by binding specific *N*-glycans (Fiedler and Simons, 1995). This hypothesis was strengthened by the finding that *N*-glycans can act as apical sorting signals for some proteins (Scheiffele *et al.*, 1995; Gut *et al.*, 1998). However, recent work provides substantial evidence that endog-

[V] Online version of this essay contains video material for the figures. Online version is available at www.molbiolcell.org.

Present addresses: §Research Program Tumor Cell Regulation, German Cancer Research Center DKFZIm Neuenheimer Feld, 280D-69120 Heidelberg, Germany; ‖Massachusetts General Hospital Cancer Research Center, 149-7202 13th St., Charlestown, MA 02129.

¶ Corresponding author. E-mail address: jwhite@helix.mgh.harvard.edu.

# These authors contributed equally to this work.

Abbreviations used: BFA, brefeldin A, CFP, cyan fluorescent protein; ERGIC, ER-Golgi intermediate compartment; FP, fluorescent protein; GFP, green fluorescent protein; KDELR, KDEL receptor; SP, spacer (15 amino acid insert); TCR, transmembrane cargo receptor; TGN, trans-Golgi network; VIP, vesicular integral membrane protein; VSV-G, vesicular stomatitis virus glycoprotein; YFP, yellow fluorescent protein.

enous VIP36 is present in the early secretory pathway in a variety of cell types, including Madin-Darby canine kidney cells (Füllekrug *et al.*, 1999a), suggesting that it was a contaminant in the *trans*-Golgi network-derived vesicle preparations, and implying that it functions in early secretory events. The different findings for VIP36 localization (Fiedler *et al.*, 1994; Füllekrug *et al.*, 1999a), together with its lectin activity (Fiedler and Simons, 1996; Hara-Kuge *et al.*, 1999), could be explained by positing that VIP36 acts as a trafficking chaperone or cargo receptor, which associates with glycosylated secretory cargo early in the secretory pathway, and then accompanies it to a later site, where post-Golgi transport carriers (TCs) are formed, leading to the speculation that VIP36 may be transiently redistributed by high levels of secretory cargo. Because the localization of VIP36 determines its site of function, and it is related to a demonstrated cargo receptor (Nichols *et al.*, 1998; Vollenweider *et al.*, 1998; Appenzeller *et al.*, 1999), it is critical to determine precisely where along the secretory pathway VIP36 associates with cargo-containing transport structures, and at what point cargo and VIP36 separate.

Generally, transmembrane cargo receptors (TCRs) are maintained in the secretory pathway by rapid recycling. TCRs in the early secretory pathway of mammalian cells include ERGIC-53 (Schweizer *et al.*, 1990; Lahtinen *et al.*, 1992), the KDEL-receptor (KDELR; Lewis *et al.*, 1990; Semenza *et al.*, 1990; Pelham, 1991), and the p24 family of proteins (Stamnes *et al.*, 1995; Sohn *et al.*, 1996; Nickel *et al.*, 1997; Füllekrug *et al.*, 1999b; Gommel *et al.*, 1999). Localization studies in fixed cells indicates endogenous VIP36 should also be included in this class, but recycling of VIP36 has not been directly demonstrated. Cargo receptors organize certain cargo proteins into distinct anterograde or retrograde transport carriers, and either facilitate (ERGIC-53 and p24/Emp24p; Nichols *et al.*, 1998; Vollenweider *et al.*, 1998; Appenzeller *et al.*, 1999; Muniz *et al.*, 2000) or initiate (KDELR; Aoe *et al.*, 1997, 1998) transport when loaded with cargo. Because they only accompany cargo in one direction, either anterograde or retrograde, the rapid recycling of TCRs is critical for their function (Vollenweider *et al.*, 1998). Furthermore, their characteristic trafficking has been used to dissect the signals and molecular interactions that drive transport (Hsu *et al.*, 1992; Lewis and Pelham, 1992; Fiedler *et al.*, 1996; Campbell and Schekman, 1997; Aoe *et al.*, 1997; Aoe *et al.*, 1998; Dominguez *et al.*, 1998; Majoul *et al.*, 1998; Bremser *et al.*, 1999; Jackson *et al.*, 1999) and generate restricted localization (Schindler *et al.*, 1993; Townsley *et al.*, 1993; Itin *et al.*, 1995; Fiedler and Rothman, 1997; Kappeler *et al.*, 1997) along the secretory pathway. Despite the importance of trafficking for the function of this class of proteins, their dynamics has been examined thoroughly in only one case (Blum *et al.*, 1999), and the kinetic rates of their recycling have not been quantitated in live cells.

To examine the trafficking of VIP36, and its possibly transient association with cargo-containing TCs along the secretory pathway, we generated fusions of VIP36 and different colors of fluorescent protein (FP), allowing us to monitor VIP36 trafficking simultaneously with fluorescent secretory cargo and fluorescent recycling TCRs in live cells. Our results indicate quantitatively that VIP36 traffics with cargo only early in the secretory pathway, separating at the level of the Golgi. At moderate expression levels, the dynamics of VIP36 are consistent with recycling between the Golgi and ER, and we show recycling directly using organelle-specific photobleaching experiments, thus indicating that VIP36 traffics similarly to other TCRs. Quantitation of photobleaching recovery rates allowed us to measure directly the separate rates for Golgi → ER and ER → Golgi transport steps. A kinetic model, shown to be successful in describing intercompartmental transport events within the secretory pathway (Hirschberg *et al.*, 1998; Zaal *et al.*, 1999), allowed us to derive kinetic transport parameters from for separate VIP36 ER → Golgi and Golgi → ER transport steps. Our results provide the first direct measurements of the transport of one of the rapidly recycling components of the early secretory pathway. Altering the parameters of the model, supported by comparison with previously published kinetic constants for secretory pathway components (Hirschberg *et al.*, 1998; Zaal *et al.*, 1999), and by experiments in which transport was pharmacologically perturbed to change the kinetic parameters, leads to the hypothesis that apparently large differences in steady-state intracellular distribution may be generated by relatively subtle differences in the rate-limiting steps for transport of resident proteins.

MATERIALS AND METHODS

DNA Constructs

Cyan, green, and yellow fluorescent proteins are spectral variants based on the 10C (yellow), S65T (green), and W7 (cyan) mutants (Heim *et al.*, 1994, 1995; Heim and Tsien, 1996), with humanized codon usage and mutations to increase fluorescence at 37°C (Cormack *et al.*, 1996; Ormo *et al.*, 1996; Siemering *et al.*, 1996; Yang *et al.*, 1996). The parent vectors for all constructs were pEGFP-N1 (GenBank accession number U55762; Clontech Laboratories, Palo Alto, CA). Cyan and yellow versions of these vectors were generated as described (White *et al.*, 1999).

VIP36-SP-GFP comprises canine VIP36 (GenBank accession X76392) fused to a 16 amino acid spacer followed by green fluorescent protein (GFP). A fragment containing the VIP36 cDNA as an *Eco*RI-*Bam*HI fragment was generated by polymerase chain reaction (PCR) with the following oligos: 5′ CGC GAA TTC ACC GCC ATG GCG GCG GAA GGC TGG 3′ (forward primer) and 5′ TCC GGA TCC CCG TAG AAA CGC TTG TTC CG 3′. This fragment was inserted into the vector backbone of pKDELR-SP-GFP (below) cut with *Eco*RI-*Bam*HI, which removes the insert encoding KDELR. Cyan and yellow versions were constructed by swapping the FP coding regions from pEYFP-N1 and pECFP-N1 as AgeI-BsrGI fragments (White *et al.*, 1999).

KDELR-SP-GFP comprises human KDEL-receptor (Erd2.1) fused to a 16 amino acid spacer followed by GFP. PCR was used to generate a fragment that contained the *erd2.1* sequence (GenBank accession X55885) with an *Eco*RI site and Kozak consensus at the 5′ end, and a sequence replacing the stop codon of KDELR with a *Bam*HI site, followed by a sequence encoding the spacer (K)DLPAEQKLISEEDL(D) (replacing the *erd2.1* stop codon) and by a *Bgl*II site at the 3′ end. The primers used were 5′ TTC CGA ATT CAC CGC CAT GAA TCT CTT CCG ATT CCT GGG AGA C 3′ (forward primer) and 5′ GAT CTA GAT CTA GGT CTT CTT CGG AGA TGA GTT TCT GTT CGG CGG GGA GTG GAT CCG CTG CCG GCA AAC TCA A 3′. The resulting fragment was inserted into *Eco*RI-*Bam*HI cut pEGFP-N1 to yield pKDELR-SP-GFP. Cyan and yellow versions were constructed by swapping the FP coding regions from pEYFP-N1 and pECFP-N1 as AgeI-BsrGI fragments (White *et al.*, 1999).

Construction of the plasmids encoding VSVG3-GFP and T2-GFP have been described (Storrie *et al.*, 1998; Toomre *et al.*, 1999). Yellow and cyan derivatives of these were constructed by subcloning *Eco*RI-

*Bam*HI inserts into pEYFP-N1 and pECFP-N1, to generate pVSVG3-YFP, pVSVG3-CFP, pT2-YFP, and pT2-CFP.

VSVG3-SP-GFP is a derivative of VSVG3-GFP containing a spacer sequence between the C terminus of the VSVG ts045 protein and the N terminus of GFP (Keller *et al.*, 2000). Complementary oligos 5′ G GAT CTC CCC GCC GAA CAG AAA CGC ATC TCC GAA GAA GAC CTG 3′ (top) and 5′ G ATC CAG GTC TTC TTC GGA GAT GAG TTT CTG TTC GGC GGG GA 3′ (bottom) were designed encoding the amino acids (K)DLPAEQKLISEEDL(D) with *Bam*HI sticky ends. The top and bottom oligos were annealed by incubating 1.5 nmol of each 5 min at 95°C and cooling slowly to room temperature, and then phosphorylated and ligated into *Bam*HI-cut pVSVG3-GFP. The inserted oligo destroys the *Bam*HI site nearest to the VSVG coding region, leaving a unique *Bam*HI site. Orientation was verified by PCR. The spacer is enough to change the distribution of anterograde cargo from predominantly apical (VSVG3-FP) to predominantly basolateral (VSVG3-SP-FP; Keller *et al.*, 2000). Cyan and yellow versions were constructed by swapping the FP coding regions as AgeI-BsrGI fragments.

Tissue Culture, Transfections, and Immunofluorescence

COS cells (ATCC no. CRL-1650) and HeLa cells (ATCC no. CCL 185) were cultured in DMEM supplemented with 5% fetal calf serum, 2 mM L-glutamine, penicillin (100 U/ml), and streptomycin (100 μg/ml). PtK_2 cells (ATCC no. CCL 56) and Vero cells (ATCC no. CCL-81.1) were cultured in minimum essential medium (MEM) supplemented with 5% fetal calf serum, 2 mM L-glutamine, penicillin (100 U/ml), streptomycin (100 μg/ml), and 1× nonessential amino acids (Life Technologies, Eggestein, Germany). All transfections used a calcium phosphate protocol as described (Pääbo *et al.*, 1986).

For imaging lysosomal structures, Lysotracker (Molecular Probes, Eugene, OR) was added at 50 nM in MEM to PtK_2 cells transiently transfected with VIP36-SP-GFP. Cells were incubated 20 min in the presence of the dye, transferred to fresh, CO_2-equilibrated MEM without phenol red, and imaged at 37°C.

For live cell double-labeling experiments with fluorescent protein spectral variants, cells were transiently cotransfected with CFP and YFP-fusion protein expression constructs mixed in equal amounts by weight before transfection. Cotransfected cells expressing approximately equal levels of CFP and YFP-fusion proteins (based on relative fluorescent intensity) were imaged 18 to 36 h after removal of the transfection precipitate.

For immunofluorescence cells were fixed in 3.0% paraformaldehyde in phosphate-buffered saline (PBS). After quenching aldehyde groups with 10 mM NH_4Cl in PBS, cells were permeabilized with 0.1% saponin as described (Füllekrug *et al.*, 1999a). The 9E10 monoclonal antibodies against the myc epitope were used undiluted as in Füllekrug *et al.*, (1999a), described in Evan *et al.*, (1985). Secondary antibody was Cy3-coupled donkey anti-mouse (Dianova, Hamburg, Germany) diluted 1:1000. Coverslips were mounted in Moviol/glycerol (Merck, Darmstadt, Germany).

To immobilize moving TCs for high-resolution imaging, cells coexpressing CFP and YFP fusions were fixed in cold methanol 2 min, washed three times in PBS, and then imaged unmounted in PBS.

Live Cell Imaging, Temperature Shifts, and Drug Treatments

Cells were imaged live on the compact confocal camera (CCC) using the equipment and conditions described previously (Storrie *et al.*, 1998; White and Stelzer, 1999). For experiments with VSVG ts045-derived cargo, cells on 15-mm glass coverslips were transfected as described above for 6–12 h at 37°C in a CO_2 incubator (in the presence of calcium phosphate-DNA precipitate), washed three times in PBS, transferred to fresh medium, and incubated at 40°C in a CO_2 incubator an additional 8 to 16 h. Cargo was pulsed into the secretory pathway by transferring the coverslip to medium preequilibrated at 32°C, and then flipping the coverslip onto a slide chamber and transferring to the microscope as quickly as possible (generally 1–2 min). The recorded time at 32°C began as soon as the coverslip was removed from 40°C medium. VIP36-SP-FP localization and trafficking were not detectably affected by incubation at 40 and 32°C.

To block cargo in early secretory structures at 15°C, coverslips were transferred from 40°C to medium preequilibrated at 15°C, and then held at 15°C for 2 h, followed by live imaging or fixation in cold methanol 2 min (as above). To block VIP36-SP-FP transfected alone or with KDELR-SP-FP, cells incubated for 12–24 h at 37°C (after washing transfection precipitate) were shifted to 15°C for 2 h, and then fixed in cold methanol or imaged live.

Brefeldin A was added at 5 μg/ml for 30 min at 37°C where indicated. Nocodazole was added at 20 μM at 37°C for various times as indicated. Cells were treated with AlF_4^- by diluting fresh aliquots of aqueous 5 mM NH_4AlSO_4 and 500 mM aqueous KF 1:100 in MEM tissue culture medium for a final concentration of 50 μm AlF_4^- in the presence of excess F^-. In organelle-specific bleaching experiments, the bleaching protocol was started within 5 min of adding AlF_4^-, and recovery monitored for no more than ~70 min of treatment.

Image Processing and Quantitation of VIP36-SP-FP Trafficking Elements

All image processing was performed on a Macintosh computer by using the public domain NIH Image program version 1.62 (developed at the U.S. National Institutes of Health and available on the Internet at http://rsb.info.nih.gov/nih-image/). Sequential 8-bit images from the CCC were combined into stacks and animated to produce greyscale movies after subtracting the background signal from a nonfluorescent area of the image (the first 15–18 intensity values were background at the detector settings routinely used). Movies were displayed with nonlinear lookup tables (gamma-corrected), adjusted as necessary for variations between display monitors and ambient light conditions. Movies are sometimes displayed as two- or three-frame running averages (mean pixel value); we consider this valid when the movies are played at a rate at which the eye cannot distinguish single frames (>15 frames/s). Running averages were always compared with unprocessed movies to avoid displaying averaging artifacts (readily distinguishable "trailing" of a moving structure). Eight-bit movies from two channels were saved in QuickTime format and overlaid to produce 16- or 24-bit color movies in Adobe Premier. All image-processing steps were performed on uncompressed data. Movies were compressed for final display by using the QuickTime video codec. NIH Image macros used for data processing are available upon request. Adobe Photoshop 5.02 and Illustrator 8.01 were used to prepare final figures.

Quantitation of VIP36-SP-GFP Trafficking Elements and Coincidence with Cargo

To quantitate trafficking elements in movies of VIP36-SP-GFP dynamics (Figure 4), 266 separate elements in 18 independent cells) were identified by eye, categorized as either a blob or a tubule, and followed frame by frame for as many frames as possible. If a blob extended into a tubular structure, it was still categorized as a blob. An edge detection filter was sometimes used to facilitate identification of discreet elements. Tracking was facilitated by an NIH Image macro, which calculated the distance and speed the element moved between frames. The average speed of an element displayed in Figure 4 was calculated from the frame-by-frame data.

VIP36-SP-FP coincidence with secretory cargo in TCs was quantitated blind as follows. First, a number of two-color movies of cells coexpressing cargo and VIP36-SP-FP were taken by one experimenter starting at various times after shift from 40°C, or after first

incubating at 15°C for 2 h. The movies were presented to the scorer, who was not told which channel corresponded to which protein. TCs in the movies were identified by eye and scored for the presence of only CFP signal, only YFP signal, or both. Both CFP/YFP combinations were used, VIP36-SP-CFP with YFP-labeled cargo and VIP36-SP-YFP with CFP-labeled cargo, and movies were presented to the scorer randomly. After scoring, the CFP or YFP signal was assigned to the protein, either VIP36-SP-FP, or to cargo.

Kinetic Model

To model the transport processes of recycling between the Golgi and ER, we assumed the simplest case of a two-compartment system with constant fractional transfer coefficients (Jacquez, 1972). The ER and Golgi are assumed to be homogeneous and well mixed, reasonable assumptions because transmembrane proteins diffuse rapidly within these organelles (Cole *et al.*, 1996; Ellenberg *et al.*, 1997; Sciaky *et al.*, 1997; Rolls *et al.*, 1999). It is also assumed that the system is closed, that is, no material is added or removed from the system during the course of the experiment. To ensure this assumption was valid, cycloheximide was added to inhibit new protein synthesis, and we monitored degradation in the absence of new protein synthesis in separate control experiments (online data). Because bleaching is restricted to local changes in the fluorophore (Tsien and Waggoner, 1995), not the overall conformation of the fusion protein, we assume that the transport properties of bleached VIP36-SP-FP are the same as unbleached. Transfer between the ER and Golgi is represented by the fractional transfer coefficient k, defined as the fraction of the material (VIP36-SP-GFP) originating from the compartment transferred per unit time (Jacquez, 1972).

$$\mathrm{ER} \underset{k_{(G\rightarrow ER)}}{\overset{k_{(ER\rightarrow G)}}{\rightleftharpoons}} \mathrm{Golgi} \tag{1}$$

The coefficients $k_{(\mathrm{ER}\rightarrow \mathrm{G})}$ and $k_{(\mathrm{G}\rightarrow \mathrm{ER})}$ represent the fraction of VIP36-SP-FP transported between the ER and Golgi per unit time, and may encompass a number of molecular and cellular events. Both transport steps are modeled as first order processes. If $x_{\mathrm{ER}}(t)$ and $x_{\mathrm{G}}(t)$ denote the fraction of VIP36-SP-FP in the ER and Golgi at time t, then the rate of change of VIP36-SP-FP in the ER is the sum of material lost from ER → Golgi transport and gained from Golgi → ER transport,

$$\frac{\mathrm{d}x_{\mathrm{ER}}(t)}{\mathrm{d}t} = -k_{ER}x_{ER}(t) + k_G x_G(t), \tag{2}$$

abbreviating $k_{(\mathrm{ER}\rightarrow \mathrm{G})}$ and $k_{(\mathrm{G}\rightarrow \mathrm{ER})}$ as k_{ER} and k_{G}, respectively. Equation 2 describes a linear first order process and is the same rate equation that, for example, governs a first order chemical reaction. Because the system is closed, the total amount of VIP36-SP-FP in the system is fixed at all times, thus

$$x_{ER}(t) + x_G(t) = S = 1. \tag{3}$$

S is set to 1, expressing x in terms of total material in the cell. Then eq. 2 may be rearranged to

$$\frac{\mathrm{d}x_{\mathrm{ER}}(t)}{\mathrm{d}t} = k_G - (k_{ER} + k_G)x_{ER}(t). \tag{4}$$

A real solution of this first order differential equation is

$$x_{ER}(t) = x_{ER}(0)e^{-(k_{ER}+k_G)t} + \frac{k_G}{k_{ER}+k_G}(1 - e^{-(k_{ER}+k_G)t}), \tag{5}$$

where $x_{\mathrm{ER}}(0)$ is the initial fraction following bleaching. We define X_{ER} to be the fraction of material in the ER at steady state, after a long recovery period. Assuming full recovery, this is the same as the prebleach steady-state fraction:

$$X_{ER} = \lim_{t\rightarrow\infty} x_{ER}(t) = \frac{k_G}{k_{ER}+k_G}. \tag{6}$$

At steady state, the ER → Golgi flux and Golgi → ER flux are the same

$$\frac{\mathrm{d}x_{\mathrm{ER}}(t)}{\mathrm{d}t} = \frac{\mathrm{d}x_{\mathrm{G}}(t)}{\mathrm{d}t}. \tag{7}$$

Substituting eq. 2 and the analogous expression for the rate of flux from the Golgi, into eq. 7, recalling that the system is at steady state (eq. 6), leads to

$$\frac{k_{ER}}{k_G} = \frac{X_G}{X_{ER}}. \tag{8}$$

Equations 3 and 8 can be used to express eq. 5 in terms of k_{G} and X_{ER}

$$x_{ER}(t) = x_{ER}(0)e^{-\frac{k_G}{X_{ER}}t} + X_{ER}(1 - e^{-\frac{k_G}{X_{ER}}t}). \tag{9}$$

Experimentally, $x_{\mathrm{ER}}(t)$ was plotted and eq. 9 was fit to the data, fitting simultaneously for t, $x_{\mathrm{ER}}(0)$, k_{G}, and X_{ER}. Such an experiment indicates the transfer coefficient from Golgi to ER by watching the pool of ER fluorescence recover from bleaching. An expression corresponding to eq. 9 can be derived for $x_{\mathrm{G}}(t)$ in terms of k_{ER} and X_{G} and fit to the Golgi bleaching data.

$t_{1/2}$ *and Exchange Times*

A theoretical transport half-time, $t_{1/2,\mathrm{ER}}$, can be defined by assuming full recovery from a complete bleach. In the case of $t_{1/2,\mathrm{ER}}$, the bleach would remove all Golgi fluorescence. In this case, the initial prebleach value is zero

$$x_{ER}(0)e^{-\frac{k_G}{X_{ER}}t} = 0 \tag{10}$$

and at time $t_{1/2,\mathrm{ER}}$, the fluorescence has reached half of the full recovery (steady-state) fluorescence

$$x_{ER}(t_{1/2,ER}) = \tfrac{1}{2}X_{ER}. \tag{11}$$

Substituting eq. 10 and 11 into eq. 9 and solving for $t_{1/2,\mathrm{ER}}$,

$$t_{1/2,ER} = \ln(2)\frac{X_{ER}}{k_G}. \tag{12}$$

A corresponding expression can be derived for $t_{1/2,\mathrm{Golgi}}$. The value $t_{1/2,\mathrm{ER}}$ represents the time it takes recovery of the Golgi to recover halfway, assuming the Golgi is initially completely empty. Experimentally, bleach efficiencies are never 100%, so such a condition is never achieved, but the $t_{1/2}$ values serve as a useful basis for comparison. Similarly, exchange times are the inverse of the rate constants, and indicate the amount of time for all of the fluorescent material in a compartment to exchange.

Organelle-Specific Bleaching Experiments and Bleach Recovery Quantitation

A volume encompassing either the Golgi or ER was defined using the irregular region functions on the CCC. The region was set in a plane of focus where the Golgi was clearly defined, the upper and lower Z-limits were then set, and a Z-series was taken at 1-μm intervals to define the volume. At least one and often three prebleach Z-series were taken at imaging power (~10–40 μW) and pixel dwell times (10–20 μs) to allow quantitation of prebleach steady-state distributions. The volume was then bleached by scanning through the Z-series at 100% power and longer pixel dwell times (up to 50 μs). Typically, six to eight sections were

Table 1. Organelle fractions return to steady-state after organelle-specific photobleaching

Condition	Steady state fraction (%) ER	Golgi
Prebleach[a,b]	87.0 ± 2.3	13.0 ± 2.3
ER bleach recovery[c] (n = 10)	87.8 ± 3.0	12.2 ± 3.0
Golgi bleach recovery[c] (n = 9)	87.0 ± 3.9	13.0 ± 3.9
Average recovery[b,d]	87.3 ± 1.7	12.7 ± 1.7

Intervals are ± 90% confidence.

[a] Steady-state fractions from the combined average of the prebleach stacks for the ER bleach and Golgi bleach experiments (Table 1).

[b] Not significantly different at $P \geq 0.05$, Student's t test.

[c] Steady-state fractions derived from fitted recovery curves (see MATERIALS AND METHODS).

[d] Average of values derived from fitted recovery curves to ER bleach and Golgi bleach experiments combined.

required to bleach the Golgi, and two to three for the ER. Illumination was reset to the prebleach imaging intensity and recovery monitored by imaging the volume of the cell every 10 to 20 s for 30 to 40 min. The CCC was programmed to automatically execute the prebleach-bleach-recovery protocol for controlled, reproducible timing. The effectiveness of the bleaching protocol was verified and quantitated with control experiments on fixed cells (online data). Only cells expressing moderate levels of VIP36-SP-FP that had a compact, well-defined Golgi morphology were used in organelle bleaching experiments. Bleach experiments were carried out in the presence of 100 μg/ml cycloheximide to ensure that no fluorescence was preferentially gained by the ER compartment during the experiment due to new protein synthesis.

Series of Z sections were quantitated with NIH Image by defining Golgi and ER regions in a single section (bounded by the bleach region), adding all pixel intensities within the regions, and subtracting background fluorescence (the total intensity from a region of equal area outside of the cell). The background-subtracted values for all sections were added to yield the total fluorescence intensities for the ER, Golgi, and cell volumes. The Golgi and ER intensities were normalized to total cell fluorescence to give a partial organelle fraction (x_{ER} or x_G). Expressing Golgi and ER values as partial organelle fractions eliminates possible effects due to bleaching caused by imaging over long recovery periods, and effects due to slight changes in focus or variability in imaging from stack to stack (due, for example, to slight fluctuations in laser power caused by temperature changes in the room). Background subtraction is essential when expressing Golgi and ER content as partial fractions. The partial organelle fractions from the prebleach stacks gave the steady-state ER-Golgi distribution of VIP36-SP-FP (Table 1).

Partial organelle fractions were plotted against time of recovery (Figure 7, right) in Kaleidagraph 3.0.5. Equation 9 or the equivalent equation for Golgi recovery was fit to the recovery data. Considering an ER bleach as an example, the model was simultaneously fit for the initial prebleach value, $x_{ER}(0)$, the partial fraction of the ER (source compartment), X_{ER}, the first order ER → Golgi rate constant, k_G, and time, t, by using reasonable experimental values as initial parameters for an iterative, least-squares fit. Regression coefficients (r) for the fits were typically >0.9.

RESULTS

VIP36-SP-FP Localization and Behavior in the Early Secretory Pathway

To visualize the intracellular trafficking and dynamics of VIP36, we fused an FP (green fluorescent protein or its cyan or yellow variants, CFP and YFP) to the C terminus of VIP36 (Figure 1A). Because VIP36 contains putative trafficking signals in its cytosolic tail (see DISCUSSION), we included a 15 amino acid spacer (SP) between VIP36 and the FP to relieve possible steric constraints, yielding VIP36-SP-FP (Figure 1A). When transiently expressed at moderate levels (judging by relative fluorescence intensity) in COS, PtK_2, HeLa, and Vero cells, VIP36-SP-FP localized to Golgi and ER structures and small punctate structures in the cell periphery associated with the ER. Figure 1B shows a typical distribution in a COS cell. At high expression levels, we also observed VIP36-SP-FP at the plasma membrane (our unpublished results), consistent with previous results (Fiedler *et al.*, 1994). Coexpression of VIP36-YFP with the fluorescent Golgi protein T2-CFP (Storrie *et al.*, 1998) (online data) and secretory cargo (see Figure 5) indicates that the compact structures next to the nucleus are Golgi membranes. VIP36-SP-FP failed to show colocalization with the lysosomal dye Lysotracker in live cells, indicating the fusion protein was not transported to this compartment for degradation (our unpublished results). Thus, at moderate expression levels VIP36-SP-FP localizes to structures early in the secretory pathway.

To rule out that the SP-FP sequences altered the localization and trafficking of VIP36, we compared VIP36-SP-GFP and VIP36 tagged at its N terminus with the myc epitope (Fiedler *et al.*, 1994). Because VIP36-SP-FP contains the full VIP36 sequence, antibodies against native VIP36 may recognize VIP36-SP-FP, precluding unambiguous, separate detection. Myc-tagged VIP36 allowed us to reliably detect each protein separately. The small myc epitope does not observably alter the trafficking behavior or localization of VIP36 by immunofluorescence (our unpublished results; Füllekrug *et al.*, 1999a). In cells that express both proteins at moderate levels, VIP36-SP-GFP colocalized with myc-VIP36 (Figure 1C). The degree of colocalization observed between VIP36-SP-GFP and myc-VIP36 is comparable to the colocalization of two proteins differing only in the color of their FP tag, under identical imaging conditions (VIP36-SP-CFP and VIP36-SP-YFP; online data). Colocalization of VIP36-SP-GFP and myc-VIP36 does not appear to depend on the coexpression of the proteins, because their distribution is not detectably altered compared with singly transfected cells (for example, compare Figure 1, B and C). Thus, VIP36-SP-FP localized identically to myc-VIP36 in the early secretory pathway, indicating that the addition of the SP-FP sequences did not alter the localization of VIP36.

Endogenous VIP36 exhibits characteristic behavior of TCRs rapidly recycling between the ER and Golgi: colocalization with other cycling proteins, and accumulation in punctate peripheral structures after incubation at 15°C and after treatment with the drug brefeldin A (BFA; Füllekrug *et al.*, 1999a). We tested whether VIP36-SP-FP possesses these same properties. The KDELR recycles between the Golgi and ER to retrieve ER resident proteins that have leaked to the Golgi (Lewis *et al.*, 1990; Semenza *et al.*, 1990), and thus serves as a well-characterized marker of ER ↔ Golgi recy-

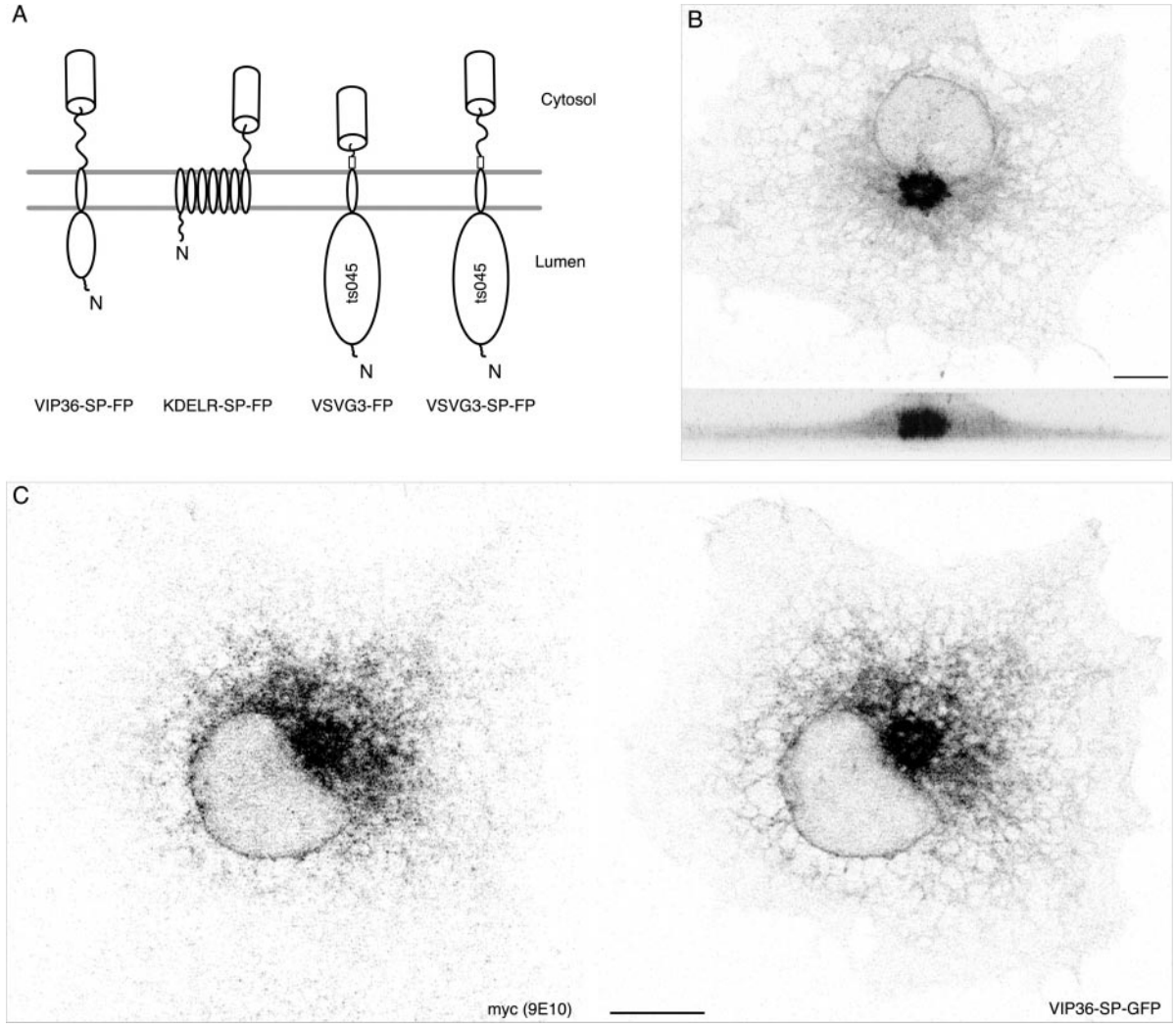

Figure 1. VIP36-SP-FP is a fluorescent marker for recycling in the early secretory pathway. (A) Fluorescent transmembrane secretory proteins used in this study. Relative orientation within the membrane, approximate domains, and placement of the fluorescent protein tag (cylinder) are indicated. All fusion proteins except VSVG3-FP contain a hydrophilic SP region (indicated by the squiggly line) between the last residue of the native protein and the FP to relieve steric hindrance between the FP and the parental protein (see DISCUSSION). VIP36 and the KDELR recycle between the ER and Golgi. VSVG fusion proteins are secretory cargo derived from the ts045 mutant of the vesicular stomatitis virus glycoprotein; they can be accumulated in the ER at 40°C and released into the secretory pathway in a synchronous pulse by shifting to 32°C. The trafficking of VSVG3-SP-FP and VSVG3-FP is indistinguishable in nonpolarized COS cells. (B) VIP36-SP-GFP distribution in a live COS cell revealed in two brightest point projections, at 0 and 90°, through a series of 20 confocal sections taken every 0.5 μm. VIP36-SP-FP localizes to the Golgi (compact structure next to the nucleus) and the endoplasmic reticulum (network throughout the cell periphery). Cells were preincubated 30 min in the presence of 100 μg/ml cycloheximide before imaging and kept in the drug during imaging. Bar, 10 μm. (C) VIP36-SP-GFP colocalizes with myc-VIP36. COS cells were cotransfected with constructs transiently expressing myc-VIP36 (Füllekrug *et al.*, 1999a) and VIP36-SP-GFP. Myc-VIP36 was detected with 9E10 monoclonal antibody and Cy3-coupled secondary; VIP36-SP-GFP signal is from the intrinsic GFP fluorescence. Shown are individual channels of single confocal sections. The online data show a color overlay and comparison of the two channels. Bar, 10 μm.

cling. VIP36-SP-FP colocalizes with an FP fusion to the KDEL-receptor, KDELR-SP-FP (White *et al.*, 1999; White and Stelzer, 1999) in live and fixed cells (Figure 2A; online data), including small punctate structures in the periphery that are closely associated with the ER (Figure 2A, insets). The observed colocalization is comparable to the colocalization of coexpressed VIP36-SP-CFP and VIP36-SP-YFP (online data). Proteins that rapidly recycle between the ER and early Golgi, such as KDELR and ERGIC-53 (Hauri *et al.*, 2000; Itin *et al.*, 1995; Tang *et al.*, 1995), redistribute to punctate structures in the cell periphery upon incubation at 15°C. After 2 h at 15°C, VIP36-SP-FP accumulates in such punctate structures in the cell periphery (Figure 2B) together with KDELR-SP-FP (Figure 2C). Rapidly recycling TCRs also redistribute to peripheral punctate structures upon treatment with BFA (Lippincott-Schwartz *et al.*, 1990; Saraste and Svensson, 1991;

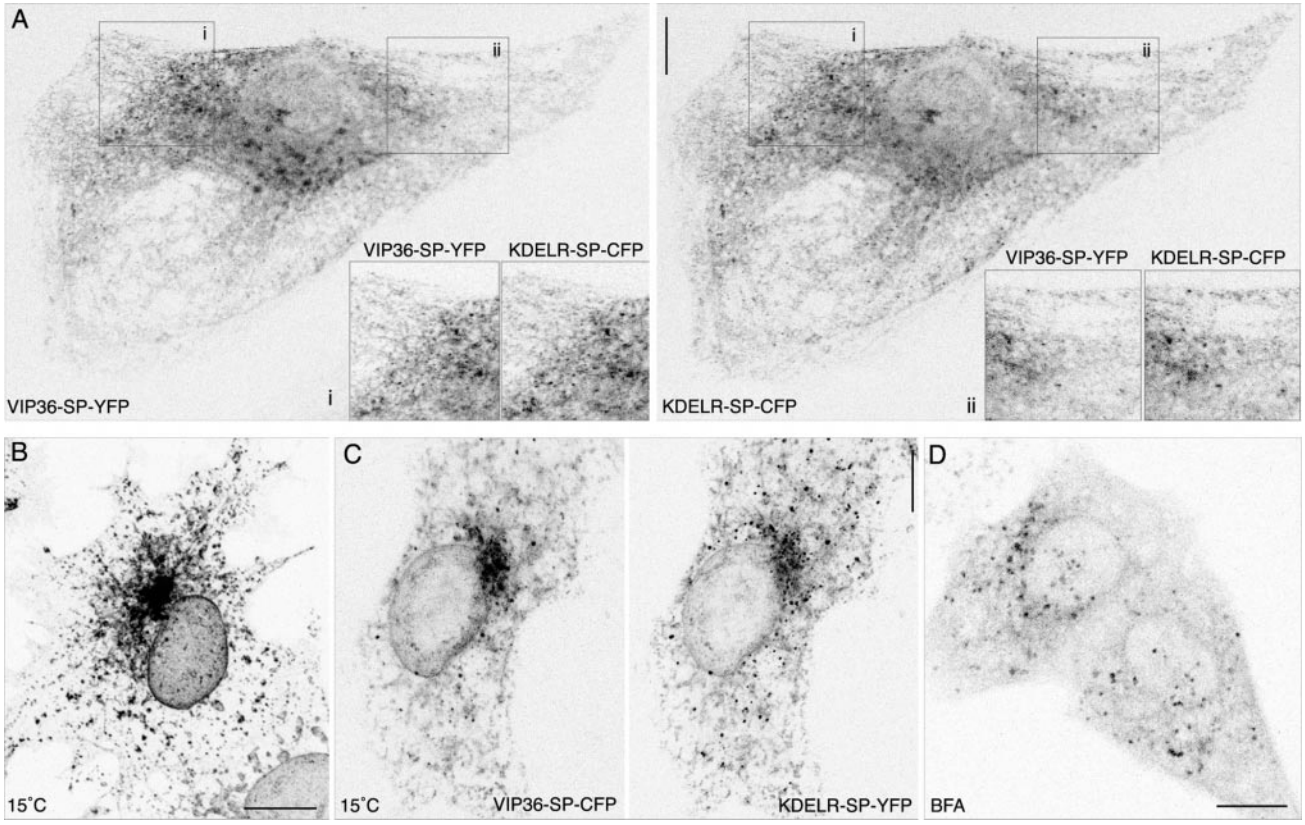

Figure 2. VIP36-SP-FP shows localization and behavior characteristic of a protein recycling in the early secretory pathway. (A) VIP36-SP-FP colocalizes with the early secretory marker KDELR-SP-FP. PtK_2 cells coexpressing KDELR-SP-CFP and VIP36-SP-YFP at 37°C were fixed in cold methanol for 2 min and mounted in PBS for high-resolution imaging. Colocalization is most apparent in peripheral punctate structures associated with the ER. Insets show regions ***i*** and ***ii*** enlarged twofold. The reciprocal FP combination (KDELR-SP-YFP and VIP36-SP-CFP) were imaged with identical results. The online data show a color overlay and comparison of the two channels. Bar, 10 μm. (B) Incubation at 15°C redistributes VIP36-SPFP to peripheral punctate structures. COS cells transiently expressing VIP36-SP-GFP were shifted from 37 to 15°C for 2 h in the presence of 100 μg/ml cycloheximide, fixed, and mounted in PBS for high-resolution imaging. Peripheral punctate structures are visible at 37°C (A) but become more prominent after incubation at 15°C. Bar, 10 μm. (C) VIP36-SP-FP accumulates together with KDELR-SP-FP in peripheral structures upon a 15°C block. COS cells transiently coexpressing VIP36-SP-CFP and KDELR-SP-YFP were incubated 2 h at 15°C in the presence of 100 μg/ml cycloheximide, fixed in cold methanol for 2 min, and mounted in PBS for imaging. The reciprocal FP combinations (KDELR-SP-CFP and VIP36-SP-YFP) were imaged with identical results. The online data show a color overlay and comparison of the two channels. Bar, 10 μm. (D) Treatment with brefeldin A redistributes VIP36-SP-FP to peripheral punctate structures. Cells transiently expressing VIP36-SP-GFP were incubated 30 min in 5 μg/ml BFA at 37°C. Golgi structures containing VIP36-SP-GFP disappear, and peripheral structures in the cell periphery become prominent. Bar, 10 μm.

Tang *et al.*, 1995; Füllekrug *et al.*, 1999b), Figure 2D demonstrates that VIP36-SP-FP shows this behavior as well. Because VIP36-SP-FP exhibits features characteristic of other recycling proteins, we conclude that VIP36-SP-FP most likely recycles between the Golgi and ER.

Typically, punctate structures that form after incubation at 15°C are enlarged pre-Golgi carriers responsible for the transport of newly synthesized anterograde secretory cargo from the ER to the Golgi (Presley *et al.*, 1997; Scales *et al.*, 1997). To verify that the punctate structures in which VIP36-SP-FP accumulated were indeed enlarged pre-Golgi carriers, we examined cells coexpressing VIP36-SP-FP and anterograde secretory cargo, either VSVG3-FP or VSVG3-SP-FP. FP fusions to the VSVG ts045 protein accumulate in the ER at 40°C due to a temperature-sensitive folding defect (Gallione and Rose, 1985; Presley *et al.*, 1997; Scales *et al.*, 1997; Toomre *et al.*, 1999). Shifting from 40 to 15°C arrests cargo in pre-Golgi carriers coated with COPI coatomer complex (Presley *et al.*, 1997; Scales *et al.*, 1997) together with recycling proteins such as KDELR (Tang *et al.*, 1995), ERGIC-53 (Saraste and Svensson, 1991; Tang *et al.*, 1995), p24 family members (Blum *et al.*, 1999; Füllekrug *et al.*, 1999b; Gommel *et al.*, 1999), and endogenous VIP36 (Füllekrug *et al.*, 1999a). We incubated COS cells coexpressing VIP36-SP-FP and VSVG3-SP-FP at 40°C, shifted them to 15°C for 2 h, and then fixed them for high-resolution confocal imaging. Both proteins accumulated in punctate structures that were closely associated with the ER network (Figure 3). This result provides evidence that VIP36-SP-FP traffics in pre-Golgi anterograde transport carriers that become enlarged at 15°C. Colocalization of VIP36-SP-FP with cargo blocked in the early secretory pathway is entirely consistent with both endogenous

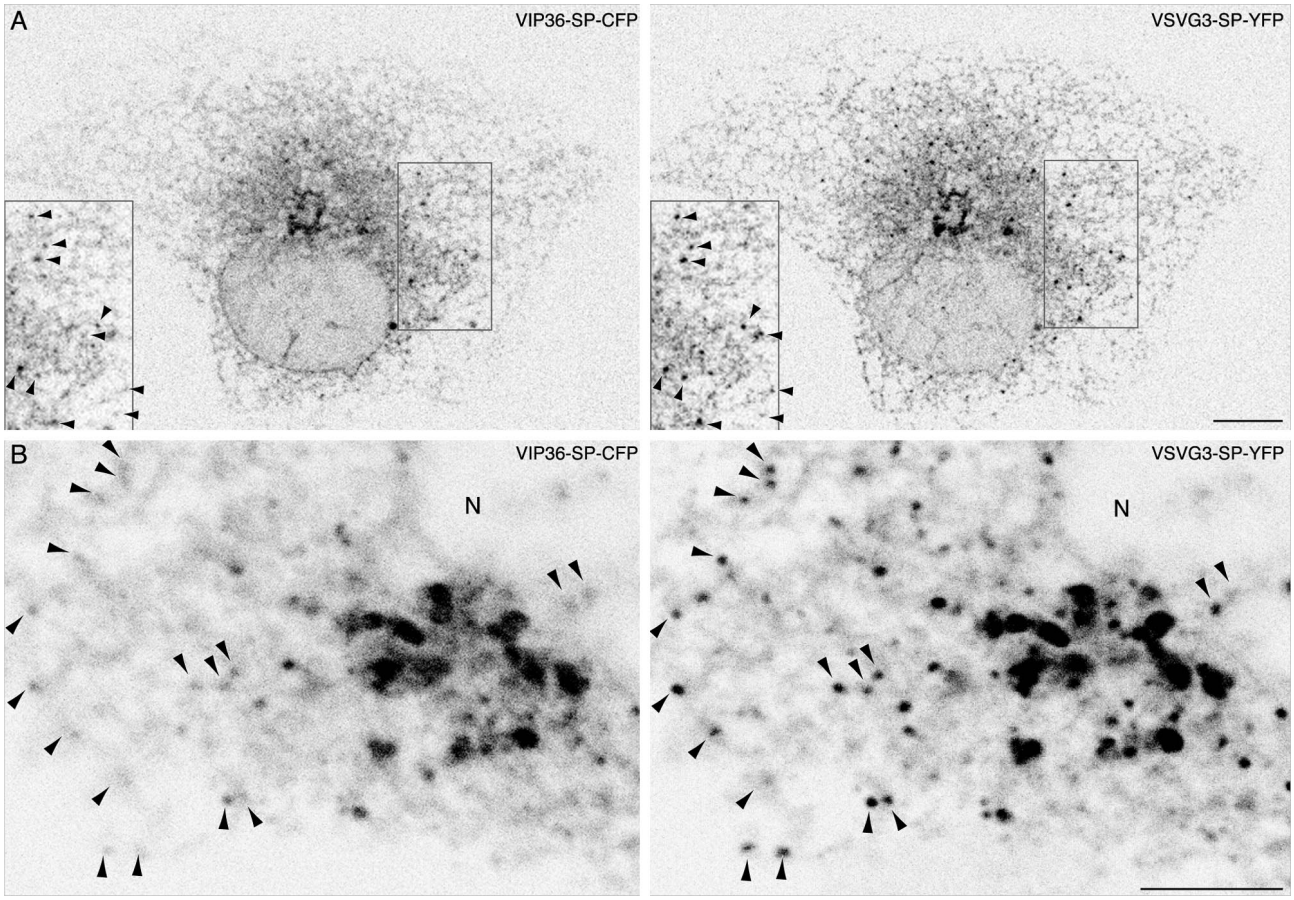

Figure 3. VIP36-SP-FP colocalizes with cargo blocked early in the secretory pathway at 15°C. The online data show a color overlay and comparison of the two channels for A and B, and an analysis of cross talk. (A) VIP36-SP-FP accumulates with cargo in pre-Golgi transport carriers in the cell periphery. COS cells transiently coexpressing VIP36-SP-CFP and VSVG3-SP-YFP were incubated 6 to 12 h at 39.5°C to accumulate cargo in the ER and then shifted to 15°C for 2 h in the presence of cycloheximide to block cargo in early secretory structures. Cells were then fixed in cold methanol and mounted for high-resolution imaging in PBS. Images are individual, line-interlaced channels of single confocal sections. Inset shows the boxed region enlarged twofold. The reciprocal FP combination (VSVG3-SP-CFP and VIP36-SP-YFP) were imaged with identical results. Bar, 10 μm. (B) High-resolution, close-up view of peripheral endoplasmic reticulum and pre-Golgi structures containing both VIP36-SP-FP and secretory cargo. COS cells transiently coexpressing VIP36-SP-CFP and VSVG3-SP-YFP were treated as in A. Arrowheads indicate punctate structures that accumulate both proteins. N indicates the nucleus. Bar, 5 μm.

and myc-tagged VIP36, providing further evidence that the SP-FP tag does not affect trafficking or localization, and indicating that VIP36-SP-FP traffics in the early secretory pathway.

Dynamics of VIP36-SP-FP in Live Cells

VIP36-SP-FP recycling between the Golgi and ER is most likely mediated by TCs trafficking between the two organelles. To identify potential TCs mediating VIP36-SP-FP recycling, we examined the dynamics of VIP36-SP-GFP trafficking in live HeLa, PtK_2, and COS cells. Movies of confocal images over time reveal at least two distinct types of VIP36-SP-GFP trafficking elements: globular elements (blobs) and tubules (Figure 4; online data). Blobs coalesced in the cell periphery and tended to move inward toward the Golgi region, although blobs also moved circumferentially about the cell periphery (Figure 4). The tendency to move inward is visually apparent in movies played at higher frame rates (online data). Blobs occasionally extended into elongated tubular elements as they translocated inwards. Tubules tended to extend from the Golgi and translocate outward toward the cell periphery, but they also translocated about the periphery and sometimes moved inward (online data). We identified VIP36-SP-FP trafficking elements in 18 independent cells, classified them as blobs or tubules, tracked them as in Figure 4B, and calculated their rate of movement. Overall, blobs were more abundant than tubules (204 blobs, 62 tubules), and on average moved more slowly (0.1–0.5 μm/s). However, blob movement was saltatory (movies, online data) so this average most likely reflects less frequent movement at higher speeds. Additionally, the apparent lower frequency of tubules and their higher speed may reflect difficulty in identifying slowly translocating tubules against the tubular ER network; only rapidly moving tu-

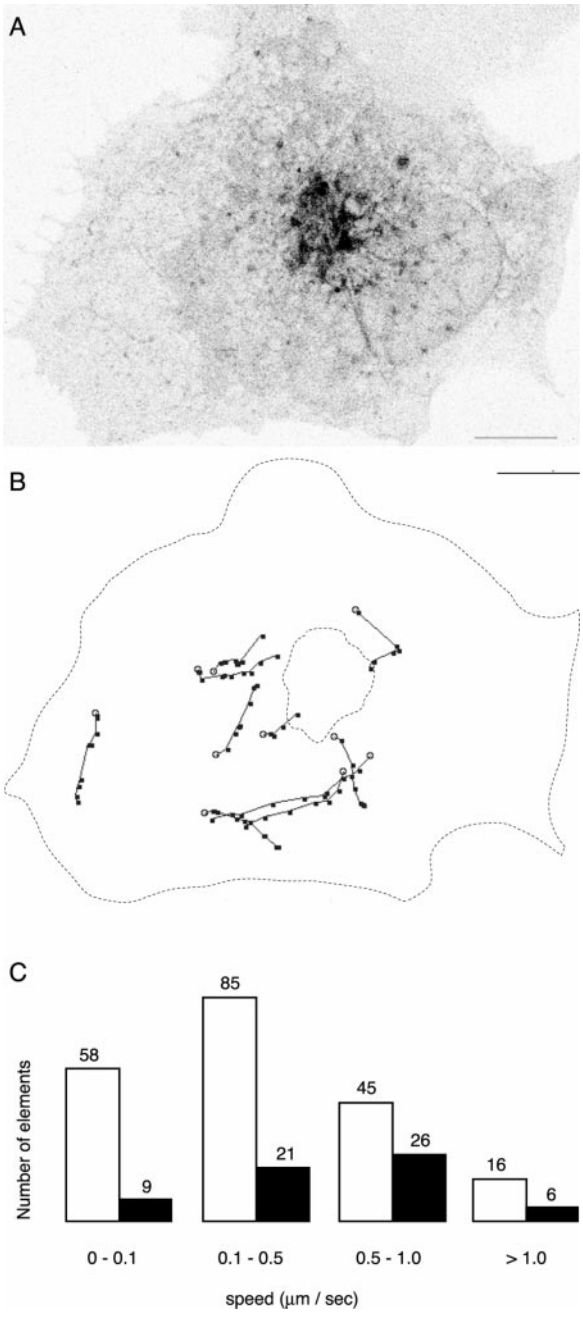

Figure 4. Dynamics of VIP36-SP-FP trafficking in live cells. (A) Representative VIP36-SP-GFP trafficking elements in a live COS cell. VIP36-SP-GFP was transiently expressed in COS cells and imaged in the presence of 100 μg/ml cycloheximide at 37°C. The image is a single frame from a movie of single confocal sections taken at the level of the ER. Trafficking structures consist of peripheral globular elements (blobs) and tubular elements (tubules). The frequency and behavior of blobs and tubules varies somewhat from cell to cell; movies in the online data depict the range of behavior observed. Bar, 10 μm. (B) Manual tracking of discreet VIP36-SP-GFP trafficking elements observed in the cell in A. The most distinct elements were tracked frame by frame. Black dots indicate the position of the element every 3.3 s. If the element extended or changed shape from frame to frame, the dot indicates the leading edge of the element in the direction of travel. Open circles indicate the initial position of the element. Scale same as A. (C) Distribution of speeds derived from manual tracking of discreet VIP36-SP-GFP trafficking elements. Trafficking elements in 18 independent cells were classified as blobs (open bars) or tubules (closed bars) and their average speed calculated (see MATERIALS AND METHODS). The exact number of elements each bar represents is indicated above the bar.

bules were easily identified by eye. We also observed variability in the ratio of blobs to tubules from cell to cell; multiple movies in the online data reflect this variability. Although the extent of directed movement is variable, the flux of tubular trafficking structures toward the periphery is consistent with a role in Golgi-to-ER transport, and the peripheral inward movement of blobs consistent with a role in ER-to-Golgi transport. The morphological similarity of the blobs to the punctate structures seen in fixed cells, which become enlarged at 15°C, accumulate anterograde secretory cargo (Figures 2 and 3), and have been shown to act as ER-to-Golgi TCs (Presley *et al.*, 1997; Scales *et al.*, 1997), strongly suggests that they are the TC for ER-to-Golgi transport of VIP36-SP-FP.

VIP36-SP-FP Traffics with Anterograde Secretory Cargo from ER to Golgi, but not Beyond

Colocalization of VIP36-SP-FP with anterograde cargo in punctate structures at 15°C indicates that it is present in ER-to-Golgi transport carriers. To determine when VIP36-SP-FP first enters cargo-containing TCs, and how far beyond early secretory structures VIP36-SP-FP traffics with cargo, we coexpressed VIP36-SP-FP together with fluorescent anterograde secretory cargo, either VSVG3-FP or VSVG3-SP-FP (Figure 1A). After accumulation in the ER at 40°C, shifting from 40 to 32°C releases a synchronous pulse of fluorescent cargo into the secretory pathway, allowing transient intermediates to be sequentially visualized (Presley *et al.*, 1997; Scales *et al.*, 1997; Hirschberg *et al.*, 1998; Toomre *et al.*, 1999).

We first examined anterograde transport at different times in fixed cells at high spatial resolution: we incubated cells coexpressing VIP36-SP-FP and VSVG3-SP-FP at 40°C, shifted to 32°C for various intervals in the presence of cycloheximide, and fixed the cells to freeze transient intermediates (Figure 5, online data show comparisons of VIP36-SP-FP and cargo channels). Fixing directly at 40°C revealed that cargo was in the ER, and that VIP36-SP-FP was localized comparably to singly transfected cells: to the ER, Golgi, and punctate elements in the cell periphery. After 10 min at 32°C, VIP36-SP-FP tended to colocalize with cargo in punctate peripheral structures, mostly likely the pre-Golgi TCs, which become enlarged at 15°C (Figure 3; Presley *et al.*, 1997; Scales *et al.*, 1997). The level of VIP36-SP-FP in the ER appeared reduced, and the VIP36-SP-FP localization in peripheral structures was most apparent at this time, indicating a change in VIP36-SP-FP distribution (Figure 5, 10-min images and comparison in online data). After 15 min at 32°C, cargo and VIP36-SP-FP colocalized tightly in the Golgi apparatus, with few peripheral structures. At later times, after 20 min, VIP36-SP-FP and cargo localized to separate peripheral punctate structures (our unpublished results; live cell movies below; online data). After 60 min at 32°C, cargo localized

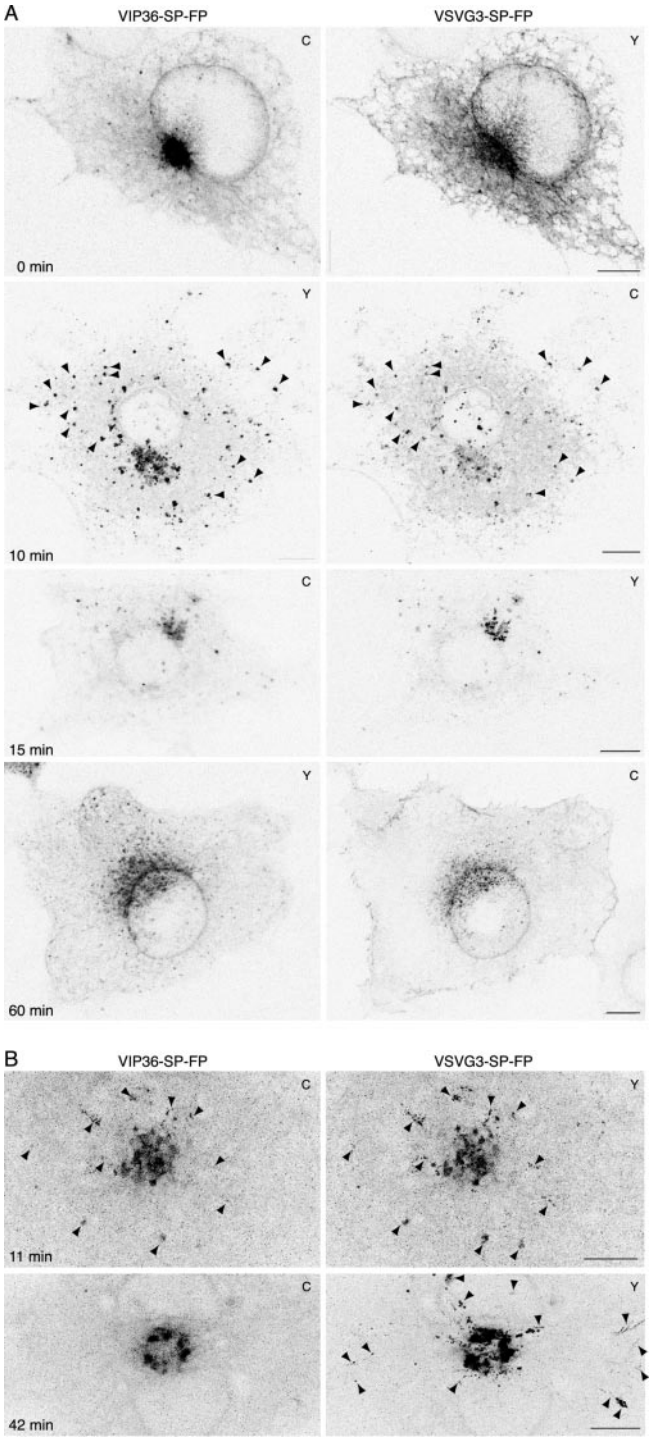

Figure 5. VIP36-SP-FP and cargo traffic together early in the secretory pathway and separate beyond the Golgi. (A) In fixed cells, VIP36-SP-FP colocalizes with cargo at early stages of secretory transport, but is in separate structures later. COS cells transiently coexpressing VIP36-SP-FP and VSVG3-SP-FP were incubated 6 to 12 h at 39.5°C to accumulate cargo in the ER and then shifted to 32°C for the indicated time in the presence of 100 μg/ml cycloheximide, fixed, and mounted for high-resolution imaging. Shown are individual, line-interlaced channels of single confocal sections taken at the level of the ER, and the difference of the two channels. C or Y in the upper right corner indicates the FP variant used in the experiment shown. Similar time points were imaged with the reciprocal color combination with identical results. The online data show a comparison and the color overlay for each set of images. Arrowheads at 10 min point out TCs that contain both proteins Bars, 10 μm. (B) In live cells, VIP36-SP-FP traffics with cargo at early stages of secretory transport, but separates later. Expression and imaging as in A, except cells were imaged live at 37°C starting at 11 or 42 min after shift to 32°C. The images are brightest point projections through all time points of a movie, which shows the positions of structures over time in a single frame (11 min, 40 frames at 11.46 s/frame; 42 min, 30 frames at 9.5 s/frame). C or Y in the upper right corner indicates the FP variant used in the experiment shown. Similar time points were imaged with the reciprocal color combination with identical results. Arrowheads at 11 min indicate TCs that contain both proteins. The online data show greyscale and color movies and additional movies at different times of transport. Arrowheads at 42 min indicate TCs that contain only cargo. Bars, 10 μm.

to the plasma membrane, and VIP36-SP-FP localized to the ER and Golgi, again a comparable localization to singly transfected cells (Figure 5A, 60 min). We often observed residual cargo in earlier structures even after longer times in the presence of cycloheximide; this pool of cargo cleared early structures slowly in our experiments, and may represent protein slowly entering the secretory pathway due to severe misfolding. Because VIP36-SP-FP distribution appeared different during ER → Golgi transport, but not at other times (compare Figure 5A, 0, 15, and 60 min), a synchronous pulse of transport may alter VIP36-SP-FP distribution. Regardless of subtle changes in VIP36-SP-FP distribution, these observations show clearly that VIP36-SP-FP colocalized with cargo from ER exit until the cargo began to leave the Golgi apparatus.

To determine how VIP36-SP-FP entered cargo-containing structures, and to determine precisely where and how VIP36-SP-FP separated from cargo, we observed fluorescent cargo and VIP36-SP-FP together in live cells. Due to the rate of FP bleaching in moderately expressing cells (cells that showed a normal distribution of VIP36-SP-FP), we were not able to continuously image a single cell long enough to observe a complete sequence of transport from the ER to the plasma membrane, so we began movies at different times after shifting from 40 to 32°C and imaged for short, continuous periods. These movies revealed that VIP36-SP-FP and cargo coincided in ER-associated, tubular structures that coalesced into punctate pre-Golgi TCs (online data, 16-min closeup, element in lower left quadrant). These results indicate that VIP36-SP-FP coalesced into pre-Golgi TCs together with cargo, during ER exit, rather than being recruited to preexisting TCs, and thus associated with cargo-containing structures very early in the secretory pathway. These movies also showed that the punctate structures containing VIP36-SP-FP and cargo moved toward the Golgi apparatus (Figure 5B and supplementary material, 11 min), providing strong evidence that the VIP36-SP-FP blobs are pre-Golgi anterograde TCs.

At later times after shift to 32°C, either directly from 40°C or after accumulation in pre-Golgi structures at 15°C, movies revealed that VIP36-SP-FP and cargo do not coincide in dynamic TCs (Figure 5B and supplementary material, 42 min and later). At times after 30 min at 32°C, we observed

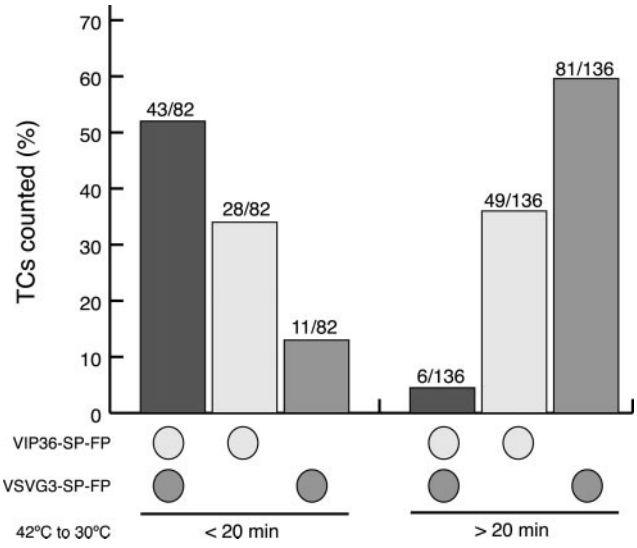

Figure 6. VIP36-SP-FP and VSVG3-SP-FP cargo are found together in TCs frequently at earlier stages of transport, but infrequently at later stages. COS cells transiently coexpressing VIP36-SP-FP and VSVG3-SP-FP were incubated 6 to 12 h at 39.5°C to accumulate cargo in the ER and then shifted to 32°C for various times in the presence of 100 μg/ml cycloheximide. Movies were taken at frame rates of 3 to 10 s/frame (see online data for representative movies). In the movies, individual TCs, defined as globular structures in the cell periphery (arrowheads in Figure 5) were scored blind for detectable CFP signal, YFP signal, or both. CFP and YFP signals were subsequently assigned to VIP36-SP-FP and VSVG3-SP-FP. Based on the timing of VSVG3-SP-FP transport, cargo-containing TCs observed earlier than 20 min are pre-Golgi carriers, those later than 20 min are primarily post-Golgi carriers. We quantitated 218 TCs in 38 cells: 82 TCs in 23 cells before 20 min and 136 TCs in 15 cells after 20 min.

anterograde TCs leaving the Golgi, but these post-Golgi TCs did not accumulate VIP36-SP-FP, although both proteins were present at high levels in Golgi structures (online data, movies starting at 42, 56, and 65 min). The movie starting at 50 min after shift to 32°C from a 15°C block shows two TCs exiting from a Golgi element. The element itself contains high levels of both cargo and VIP36-SP-FP, but after exit the TCs do not contain detectable VIP36-SP-FP (online data). Thus, subjective observations from a number of movies indicated that VIP36-SP-FP trafficked together with cargo early in the secretory pathway and then separated within the Golgi, so that post-Golgi carriers did not contain VIP36-SP-FP.

To quantitate these observations, 218 TCs in 38 cells were scored blindly for the presence of only VIP36-SP-FP, only cargo, or both (Figure 6). In our experiments, by 20 min at 32°C most cargo had emptied from the ER and accumulated to high levels in the Golgi, but had not yet begun to exit the Golgi in post-Golgi carriers. Thus, movies before 20 min most likely represent pre-Golgi transport, and after 20 min most likely represent post-Golgi transport. Before 20 min, 52% (43 of 82) of TCs contained both proteins, but in movies taken after 20 min only 4% (6 of 136) of TCs contained both proteins. There was a greater proportion of TCs containing VIP36-SP-FP (both with and without cargo) at early times of transport: before 20 min, 86% (71 of 82) of the TCs counted contained VIP36-SP-FP, but after 20 min, only 40% (55 of 136) of the TCs contained VIP36-SP-FP. The correlation between increased number of VIP36-SP-FP TCs and cargo-containing TCs, together with the increased frequency of colocalization during ER → Golgi transport suggests that VIP36-SP-FP may be recruited to pre-Golgi carriers. Together, these quantitative results verify our subjective observations and show that VIP36-SP-FP and cargo traffic together in pre-Golgi carriers, but post-Golgi carriers do not contain detectable VIP36-SP-FP.

Kinetics of VIP36-SP-FP Exchange between Golgi and ER Quantitated with Organelle-Specific Photobleaching

The pattern of VIP36-SP-FP localization under different conditions (Figures 2 and 3), is consistent with the behavior of endogenous VIP36 (Füllekrug *et al.*, 1999a), and support the idea that it recycles between the ER and Golgi, but does not show recycling directly. To demonstrate VIP36-SP-FP recycling in live cells we performed organelle-specific photobleaching experiments. Using the region functions on our confocal microscope, we photobleached a volume encompassing either the Golgi (Figure 7A) or the ER (Figure 7B), through the entire depth of the organelle (online data). Fluorescence recovered into the bleached volume over time (Figure 7, recovery panels), indicating transport from the unbleached to the bleached organelle.

We quantitated the fluorescence recovery into the bleached volume (Figure 7, right) and derived kinetic rate constants based on a linear, first order model for transport between two compartments in a closed system (see MATERIALS AND METHODS; Jacquez, 1972),

$$\mathrm{ER} \underset{k_{(G\rightarrow ER)}}{\overset{k_{(ER\rightarrow G)}}{\rightleftharpoons}} \mathrm{Golgi}.$$

This model assumes, among other things, that the rate of transport from one compartment to another is directly proportional to the amount of material in the source compartment multiplied by a coefficient, the first order rate constant (see MATERIALS AND METHODS; Jacquez, 1972). The balance of forward transport and retrograde transport determines the ratio of VIP36-SP-FP in each compartment at steady state, after long recovery periods. Similar methods have been used to analyze Golgi ↔ ER recycling of Golgi resident proteins (Zaal *et al.*, 1999) and transport of anterograde secretory cargo (Hirschberg *et al.*, 1998).

The linear, first order kinetic model fits the measured recovery data well (Figure 7, right). Regression coefficients (r) were typically >0.9. At steady state before the bleach, the ER contained 87.3 ± 1.7% and the Golgi 12.7 ± 1.7% of the total cellular fluorescence. The fit to the recovery data indicates that the ER and Golgi reestablish this steady state ratio following the bleach, and the same steady-state ratio is reestablished regardless of which organelle was bleached (Table 1). Although most of the VIP36-SP-FP is present in the ER, the fluorescence is distributed over a much greater area, so VIP36-SP-FP in the ER appears less prominent visually. These data show that there is ongoing transport of VIP36-SP-FP from Golgi to ER, and ER to Golgi, thus demonstrating recycling of VIP36-SP-FP directly in live cells.

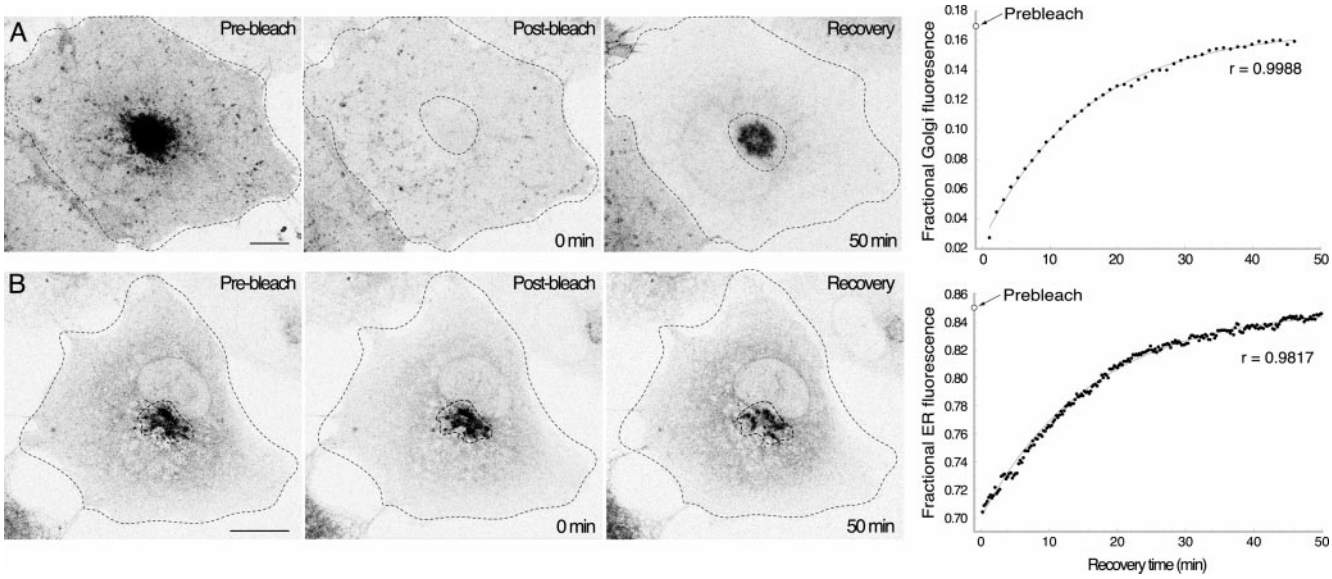

Figure 7. Organelle-specific bleaching determines the kinetic parameters of VIP36-SP-GFP exchange between the ER and Golgi. See the online data for bleach parameters and controls. (A) Golgi-specific bleach experiments directly measure the transfer of fluorescence from the ER to the Golgi. The Golgi region defined by the dotted line was selectively bleached in a COS cell transiently expressing VIP36-SP-GFP. Panels show before, immediately after, and 50 min after the bleach for a representative experiment. Images are brightest point projections through a series of confocal sections over the entire depth of the cell. The recovery of fractional Golgi fluorescence for the cell shown is plotted on the far right (see MATERIALS AND METHODS), and the fit of the kinetic model is indicated by the light gray line through the data. The prebleach fractional Golgi fluorescence is indicated on the *y*-axis. After 50 min of recovery the cell appears dimmer because fluorescence was removed by the bleach (online data). Bar, 10 μm. (B) ER-specific bleach experiments directly measure the transfer of fluorescence from the Golgi to the ER. The ER region was selectively bleached in a COS cell transiently expressing VIP36-SP-GFP. Panels show before, immediately after, and 35 min after the bleach for a representative experiment. Images are brightest point projections through a series of confocal sections over the entire depth of the cell. The recovery of fractional ER fluorescence for the cell shown is plotted on the far right (see MATERIALS AND METHODS), and the fit of the kinetic model is indicated by the light gray line through the data. The prebleach fractional ER fluorescence is indicated on the *y*-axis. Bar, 10 μm.

Kinetic rate constants can be derived from the fit to the data. They characterize the efficiency of VIP36-SP-FP transport at each step, which reflects multiple molecular and cellular events. Table 2 shows the transport rate constants derived for ER $\rightarrow$ Golgi (k_{ER}) and Golgi $\rightarrow$ ER (k_G) transport steps. For a given experiment (ER bleach or Golgi bleach), we derived a rate constant in one direction (the forward transport step) directly from the fitted curve (Table 2; see MATERIALS AND METHODS). Because the ratio of the forward and reverse transport constants is related to the steady-state ratio of VIP36-SP-FP in each compartment (see MATERIALS AND METHODS, eq. 8), we calculated the reverse transport rate constant from the forward value and the fitted steady-state fraction of VIP36-SP-GFP in the ER and Golgi (Table 2). Values for k_{ER} and k_G calculated in this manner, independently for ER bleaching and Golgi bleaching experiments, agree well, thus supporting the idea that we are measuring the reciprocal transport processes predicted by the model.

The rate constant of Golgi $\rightarrow$ ER transport was approximately sixfold greater than the ER $\rightarrow$ Golgi constant (Table 2). Accordingly, a single VIP36-SP-GFP protein spends a much longer time in the ER than in the Golgi. This time is reflected in two values, $t_{1/2}$ and the exchange time (Table 2). The $t_{1/2}$ value assumes the hypothetical case where one compartment is completely bleached, and it represents the time it takes for recovery to proceed halfway to completion (see MATERIALS AND METHODS), It is often reported to characterize first order process (Jacquez, 1972). Previously published studies report an exchange time (Hirschberg *et al.*, 1998; Zaal *et al.*, 1999), simply the inverse of the rate constant, which represents the time it takes for all of the fluorescent material in a compartment to be transported (see MATERIALS AND METHODS). Because recovery is nonlinear (Figure 7), $t_{1/2}$ and the exchange time together provide a more complete picture of the recovery process, so we report both for VIP36-SP-FP ER $\leftrightarrow$ Golgi recycling (Table 2). The exchange times indicate it take 8.5 times as long for all VIP36-SP-FP to exchange out of the ER than out of the Golgi, or 62 times as long for VIP36-SP-FP to recovery to completion in the Golgi than in the ER. Altogether, our modelling and analysis of organelle-specific photobleaching recovery provides direct evidence for ER $\leftrightarrow$ Golgi recycling of VIP36-SP-FP, and shows that a relatively simple model accounts for both its steady-state distribution and its transport characteristics.

Perturbing VIP36-SP-GFP Transport Alters Its Distribution and Kinetic Rate Constants

The model predicts that change in the distribution of VIP36-SP-GFP should be accompanied by a corresponding change in the ratio of the rate constants. To change the distribution of VIP36-SP-GFP, we treated cells with drugs known to

Table 2. Kinetic rates of VIP36-SP-GFP recycling between the Golgi and ER

	Transport rate constants (% · min^{-1})		$t_{1/2}$[a] (min)		Exchange time[a] (min)	
Experiment	ER→Golgi	Golgi→ER	ER→Golgi	Golgi→ER	ER→Golgi	Golgi→ER
ER bleach (n = 10)	1.22[b] ± 0.66	7.60[c] ± 2.24	113 ± 70	1.36 ± 0.45	178 ± 106	17.3 ± 5.0
Golgi bleach (n = 9)	1.23[c] ± 0.59	7.74[b] ± 3.14	98.1 ± 40.4	1.94 ± 0.75	160 ± 66	22.2 ± 8.6
Combined	1.22 ± 0.44	7.68 ± 1.94	105 ± 39	1.67 ± 0.45	169 ± 59	19.9 ± 5.1

Intervals are 90% confidence for the number of trials shown.

[a] Calculated for each experiment and then averaged.

[b] Transport rates calculated from the fitted curves and steady-state fraction (see MATERIALS AND METHODS).

[c] Transport rates derived directly from the fitted curve.

perturb transport. Initially, we considered cells treated with BFA and nocodazole. BFA treatment results in the explosive redistribution of the Golgi pool of VIP36-SP-GFP to the ER and punctate peripheral sites (Figure 2). Nocodazole treatment also redistributes the Golgi pool of VIP36-SP-GFP to peripheral punctate structures, with dynamics similar to the redistribution of Golgi enzymes (Storrie *et al.*, 1998), but more rapidly (within 30 min; our unpublished results). Both these treatments completely disassemble the Golgi structures and thus are equivalent to setting the ER → Golgi rate constant in the model to zero (in this case defining "Golgi" as compact structures next to the nucleus). Because they completely alter the perinuclear Golgi structure, we could not perform organelle-specific bleaching experiments to test for changes in the rate constants.

Treatment with 50 μM aluminum fluoride changed the distribution of VIP36-SP-GFP more subtly. Within 1 h of treatment, the ER:Golgi ratio changed to 66:34 ± 4% (n = 10). We avoided experiments after long periods of treatment to avoid possible toxic effects of AlF_4^-. Because AlF_4^- treatment blocks Golgi exit of anterograde cargo and inhibits diffusion of proteins within the Golgi (Cole *et al.*, 1996), we expected (Blum *et al.*, 1999) the drug to generally inhibit ER ↔ Golgi transport, resulting in smaller rate constants for both steps, so any change in the relative ER-Golgi distribution would be due to differential reduction of the rate constants. However, Golgi bleaching experiments indicated that the ER → Golgi rate constant increased to 5.53 ± 1.10%/min (n = 10), requiring a Golgi → ER constant of 12.0 ± 3.4%/min to account for the new distribution, assuming the system reaches steady state within an hour. It seems likely that cells reach a new steady state because the recovery levels off asymptotically after 60 min. Additionally, we monitored the response of unbleached cells in the same field of view during the AlF_4^- bleach experiments. In most cells (4 of 5) the VIP36-SP-GFP distribution was altered within the time it takes to add the drug and resume imaging (~3–5 min), and fluctuated by approximately ±15% about the new distribution. In one of five experiments, we saw a smooth monotonic change in the distribution, which leveled off asymptotically by 60 min. In the bleached cells, the prebleach ratios are already shifted from the 87:13 ratio of untreated cells, consistent with a rapid effect of the drug. Regardless, because the assumption of steady state is invoked only in calculating the opposing rate constant, that is, the Golgi → ER constant for a Golgi bleach, the fit to the Golgi-bleach recovery data indicates that perturbing transport indeed alters $k_{ER \to G}$.

DISCUSSION

To examine the dynamics of VIP36 trafficking and determine precisely where VIP36 separates from cargo along the secretory pathway in live cells, we established VIP36-SP-FP as an accurate marker for VIP36 in live cells. VIP36-SP-FP colocalizes with myc-VIP36 (Figure 1) and exhibits trafficking behavior characteristic of TCRs recycling in the early secretory pathway (Figures 2 and 3), including VIP36 (Füllekrug *et al.*, 1999a). We conclude that VIP36-SP-FP localization is relevant to native VIP36, thus VIP36-SP-FP trafficking reflects VIP36 trafficking in live cells. More generally, we conclude that VIP36-SP-FP trafficking is representative of TCR recycling in the early secretory pathway.

Because VIP36 contains putative trafficking signals in its C-terminal cytosolic tail, it might be expected that the C-terminal SP-FP sequences interfere with the trafficking and localization of VIP36-SP-FP. VIP36 contains the sequence KRFY at its C terminus, and in the closely related lectin ERGIC-53 (Fiedler and Simons, 1994), a similar sequence in the cytosolic tail, KKFF, contains multiple trafficking determinants (reviewed by Hauri *et al.*, 2000). In VIP36, the KR sequence is similar to dilysine ER-retrieval motifs (Jackson *et al.*, 1990; Schindler *et al.*, 1993) and could be expected to function in Golgi → ER transport by binding COPI coatomer (Kappeler *et al.*, 1997). The FY sequence is similar to diphenylalanine motifs mediating ER exit (Kappeler *et al.*, 1997; Tisdale *et al.*, 1997), and could be expected to function in ER → Golgi transport by interacting with COPII coat complex (Kappeler *et al.*, 1997). Our experience shows that the SP sequence in VIP36-SP-FP allows cytosolic signals in other proteins to be verifiably recognized. When included between VSVG and the FP in our anterograde cargo constructs, the SP allows cytosolic basolateral targeting signals in VSVG to be recognized, shifting the apical distribution of VSVG3-FP to the basolateral distribution of VSVG3-SP-FP (Keller *et al.*, 2000). Consistent with this, a construct lacking the SP between VIP36 and the FP exhibited low trafficking activity (no moving blobs or tubules) and altered localization (shifted toward the ER; our unpublished results). Thus, we posit that the SP allows putative trafficking signals in the

cytosolic tail to be recognized Additionally, the trafficking of ERGIC-53 is determined by factors other than simple sequence motifs in the cytosolic tail, including determinants in the lumenal and transmembrane domains (Kappeler *et al.*, 1997). Consistent with this, placement of the GFP at the N terminus of mature VIP36 (after the signal sequence) results in mislocalization of the fusion protein to aggregated structures in the periphery (our unpublished results). Finally, VIP36 may oligomerize, again by analogy to ERGIC-53, which forms homodimers and homohexamers (Schweizer *et al.*, 1990; Lahtinen *et al.*, 1992). All our experiments were performed with cells expressing VIP36-SP-FP at moderate levels in which endogenous VIP36 was most likely still present, so it is conceivable that hetero-oligomers between VIP36-SP-FP and endogenous VIP36 trafficked according to dominant signals in the endogenous protein, and these putative hetero-oligomers were what we visualized and measured. Regardless, our results show that VIP36-SP-FP traffics extensively (Figure 4) and does indeed efficiently recycle between the ER and Golgi, by conventional criteria (Figures 2 and 3) and by measuring the ER → Golgi and Golgi → ER steps of recycling directly (Figure 7 and Table 2; see below).

The dynamics of VIP36-SP-FP are consistent with a role in ER ↔ Golgi recycling. VIP36-SP-FP exhibited high trafficking activity in live cells (online data; Figure 6), and we observed two classes of trafficking structures: blobs and tubules (online data; Figure 6). Our data indicate that the blobs were anterograde ER → Golgi TCs, because we observed cargo in them at early times of transport, translocating toward the Golgi (online data; Figure 5; 11- and 16-min movies). They are most likely the structures that become enlarged at 15°C (Figure 2), accumulating cargo (Figure 3), consistent with previous observations of anterograde ER → Golgi TCs in live cells (Presley *et al.*, 1997; Scales *et al.*, 1997), and other observations of recycling components in live cells (Blum *et al.*, 1999). Because the tubules were the only trafficking structure observed to exit the Golgi (online data), and a Golgi → ER transport step must maintain the steady state of VIP36 (Figure 7 and Table 1), we hypothesize that at least a fraction of the tubules we observed were Golgi → ER TCs.

Our results indicate VIP36-SP-FP is restricted to the early secretory pathway. Previously, it was shown that endogenous VIP36 was present in the early secretory pathway, but did not precisely define how far along the secretory pathway VIP36 accompanied anterograde TCs (Füllekrug *et al.*, 1999a). VIP36-SP-FP trafficked together with cargo in pre-Golgi TCs (Figure 5B; online data), but VIP36-SP-FP segregated from structures containing secretory cargo at the level of the Golgi complex (Figures 5 and 6). Cargo appeared to exit the Golgi from regions at the periphery of the Golgi, that are already devoid of VIP36-SP-FP (online data; Figure 5 movies, times at 42 min and later), suggesting that VIP36-SP-FP is sorted from cargo within the Golgi complex, and perhaps indicating sorting events between early and late Golgi compartments. We observed a redistribution of VIP36-SP-FP, which correlated with the pulse of cargo (Figure 5, compare 10 and 15 min), but cargo did not induce VIP36-SP-FP to traffic in anterograde TCs beyond the Golgi, nor did it cause observable redistribution of VIP36-SP-FP to endosomes and the plasma membrane. Our experiments do not rule out that VIP36 may redistribute to post-Golgi structures in the presence of specific cargo proteins, but they do show that the presence of VIP36 in post-Golgi TCs is not a general occurrence. Thus, it is probable that the cellular function of VIP36-SP-FP is restricted to the early secretory pathway.

Our experiments do not address whether VIP36, like ERGIC-53 (Appenzeller *et al.*, 1999), functions in anterograde ER → Golgi transport. Although we observed VIP36-SP-FP and cargo together very early during ER → Golgi transport, during the coalescence of pre-Golgi TCs from the ER, it is possible that VIP36-SP-FP is itself cargo in anterograde TCs and only functions in retrograde Golgi → ER transport. This model would be consistent with the difference in dependence on Ca^{2+} for sugar binding that has been observed between ERGIC-53 and VIP36: ERGIC-53 requires Ca^{2+} to bind high-mannose sugars (Itin *et al.*, 1996; Appenzeller *et al.*, 1999), whereas VIP36 does not (Hara-Kuge *et al.*, 1999). This leads to the speculation that ERGIC-53 binds glycoproteins in the high-Ca^{2+} environment of the ER to facilitate their exit and subsequent ER → Golgi transport, and VIP36 binds glycoproteins in the Golgi to facilitate their return to the ER, perhaps as part of a quality control or degradation pathway. Because VIP36 is related to ERGIC-53, an established cargo receptor (Nichols *et al.*, 1998; Appenzeller *et al.*, 1999), and traffics similarly to recycling TCRs (Figures 2 and 3; online data), it is relevant to establish with which cargo-containing structures it associates during secretory transport. However, further localization of VIP36 function awaits identification of VIP36 ligands.

Previous work showed the presence of VIP36 the early secretory pathway, and changes in its localization in response to BFA or 15°C incubation suggested it trafficked similarly to TCRs cycling between the ER and Golgi, but did not show exchange. Here, we used organelle-specific photobleaching experiments to show both transport steps of recycling separately, directly demonstrating ER ↔ Golgi exchange of VIP36-SP-GFP. Because photobleaching most likely produces very local changes in the GFP chromophore, transport of VIP36-SP-GFP should not be perturbed by bleaching. Thus, recovery from photobleaching reflects ongoing transport that maintains the steady state of VIP36-SP-FP. This is supported by our data, because VIP36-SP-FP reestablishes the same 87/13 steady state after bleaching (Table 1), bleached material was transported out of the bleached region as unbleached material was transported in. Quantitation of photobleaching recovery allowed us to fit a simple two-compartment model to the data and provided kinetic parameters for each step of the exchange. This model is the simplest reasonable model based on morphological observations and verifiable assumptions (see MATERIALS AND METHODS). The linear, first order fractional transfer coefficients derived from the model represents the overall rate-limiting step in the transport process, and most likely encompass a number of molecular and cellular events. That is, a good fit to a simple model does not imply that the transport process itself is simple, it merely indicates that there is a rate-limiting step within the transport process that can be accurately described by a first order rate constant. The transport coefficients for ER → Golgi and Golgi → ER transport processes indicate that VIP36-SP-FP is transported from the Golgi to the ER sixfold more efficiently than from ER to Golgi (Table 2), accounting for the high proportion of VIP36-SP-FP in the ER at steady state (Table 1). The ratio of forward and reverse coefficients matches the measured

Table 3. Comparison of VIP36-SP-FP with published kinetic parameters for proteins along the secretory pathway

	Linear, first order rate constants (% · min^{-1})			Exchange time[a] (min)		
Protein	ER→Golgi	Golgi→ER	Golgi→PM	ER	Golgi	PM
VIP36-SP-GFP	1.22	7.68	n.d.	169.0	19.9	n.d.
GalTase-GFP$_3$[b]	3.60	1.80	n.d.	27.5	57.2	n.d.
VSVG-GFP[c]	2.84	n.d.	3.0	39.4	42.8	709

n.d., not detected.

[a] Exchange times for VIP36-SP-FP were calculated for each experiment and then averaged.

[b] Golgi type II resident protein (Zaal *et al.*, 1999).

[c] Secretory cargo (Hirschberg *et al.*, 1998).

steady-state distribution of VIP36-SP-FP well (Table 1; see MATERIALS AND METHODS, eq. 8), providing further support that the model explains VIP36-SP-FP transport. Quantitation of VIP36-SP-FP transport kinetics is generally important and interesting because our data indicate that VIP36-SP-FP is representative of TCRs recycling in the early secretory pathway, and the recycling of these proteins is critical for their function as receptors for different classes of cargo (Itin *et al.*, 1995; Fiedler *et al.*, 1996; Nichols *et al.*, 1998; Vollenweider *et al.*, 1998; Appenzeller *et al.*, 1999; Blum *et al.*, 1999; Bremser *et al.*, 1999; Gommel *et al.*, 1999; Moussalli *et al.*, 1999; Muniz *et al.*, 2000).

Perturbing transport should alter the kinetic rate constants and should change the relative distribution of VIP36-SP-FP if the constants are altered to different degrees. Reciprocally, a change in distribution indicates a change in the ratio of the rate constants. Treatment with aluminum fluoride, a drug that perturbs transport, altered VIP36-SP-FP distribution, so we performed organelle-specific bleach experiments to test for a corresponding change in the ER → Golgi kinetic rate constant. We were able to perform such experiments because AlF_4^- treatment did not destroy the central Golgi structure, unlike treatment with nocodazole or BFA. Rather, 1 h of treatment with 50 μM AlF_4^- shifted the distribution of VIP36-SP-GFP to an ER:Golgi ratio of ~64:34%. Golgi-bleach experiments indicated that the ER → Golgi kinetic rate constant increased from 1.22%/min to 5.53%/min, indicating that ER → Golgi transport is somehow more efficient under these conditions. Aluminum fluoride is a general activator of heterotrimeric G proteins (reviewed by Helms, 1995), inhibits COPI exchange off of membranes (Melancon *et al.*, 1987; Donaldson *et al.*, 1991; Robinson and Kreis, 1992), and inhibits intra-Golgi transport in in vitro assays (Melancon *et al.*, 1987; Helms *et al.*, 1998). In live cells it inhibits Golgi exit of anterograde cargo (Helms *et al.*, 1998; Hirschberg *et al.*, 1998) and inhibits diffusion of Golgi proteins in Golgi membranes (Cole *et al.*, 1996). The effect of AlF_4^- particularly on ER ↔ Golgi recycling in live cells has not been extensively documented; Blum *et al.* (1999) show that after 30 min of AlF_4^- treatment, the recovery of the Golgi pool of GFP-p24 is reduced, and that peripheral trafficking structures cease to move (Blum *et al.*, 1999). In our experiments, trafficking was reduced but movement did not cease (online data). Because AlF_4^- generally acts as an inhibitor, we expected it to inhibit both ER → Golgi and Golgi → ER transport steps, with the change in distribution due to differential inhibition of the different transport steps. We reconcile our the observations with the general effects of AlF_4^- by suggesting that, in AlF_4^--treated cells, transport of VIP36-SP-GFP to later regions of the Golgi is inhibited, restricting it to earlier Golgi structures or pre-Golgi structures that are more closely associated with the ER. We observed changes in Golgi structure upon AlF_4^- treatment that are consistent with this suggestion (online data). Regardless, by showing that conditions that alter transport alter both the distribution of VIP36-SP-GFP and the ER → Golgi rate constant, our experiments quantitatively verify a prediction of the model.

Comparison of the transport coefficients for VIP36-SP-FP with published values derived from similar experiments indicates that the transport coefficients for VIP36-SP-FP are within the range measured for two other proteins along the secretory pathway (Table 3); (Hirschberg *et al.*, 1998; Zaal *et al.*, 1999). Although direct quantitative comparisons cannot be made because the parameters were not derived under identical conditions, the general methods and compartmental models are similar, so it should be reasonable to make qualitative comparisons. The Golgi-resident protein GalTase-GFP$_3$ is transported from the ER to the Golgi more efficiently than VIP36-SP-FP, and returns less efficiently, as would be expected for a protein classified as a Golgi resident (Table 3) (Zaal *et al.*, 1999). When pulsed through the secretory pathway, a fluorescent anterograde cargo protein, VSVG-GFP (similar but not identical to the VSVG3-FP construct described here) exits the ER more efficiently than VIP36-SP-FP, but return of anterograde cargo from the Golgi to the ER was not detected (Hirschberg *et al.*, 1998). Golgi exit, whether initiating anterograde or retrograde transport, was most efficient for VIP36-SP-FP. Although the three proteins for which kinetic rate constants have been determined behave very differently within the secretory pathway (one localizes primarily to the Golgi, one localizes primarily to the ER, and one never reaches steady state), their transport rate constants are all within the same order of magnitude, the largest difference among the values is in fact the sixfold ratio of k_G to k_{ER} for VIP36-SP-FP. This raises the very interesting point that relatively small differences in the rate-limiting transport step for different proteins produce very large differences in their final steady-state distributions, or determine whether a protein eventually reaches steady state. This can be explored by varying the parameters of the model

within reasonable values and applying eq. 8. Thus, the difference between a Golgi resident protein and a protein that spends most of its time in the ER (Table 3), may be due to only a fewfold difference in the rate-limiting steps for anterograde and retrograde transport, perhaps manifested in a subtle advantage for entering or being excluded from certain transport carriers.

ACKNOWLEDGMENTS

We gratefully thank the CCC development team: Stephan Albrecht (DSP programming), Alfons Riedinger (software design and programming), Georg Ritter (digital hardware), Nick Salmon (software design and programming), Thomas Stefany (optics), and Reiner Stricker (analog hardware). Thanks to James Jonkman for microscopy support and technical assistance. We thank Tom Rapoport and Anne Hart for their support in the final stages of this work and Melissa Rolls for highly critical comments on the manuscript.

REFERENCES

Aoe, T., Cukierman, E., Lee, A., Cassel, D., Peters, P.J., and Hsu, V.W. (1997). The KDEL receptor, ERD2, regulates intracellular traffic by recruiting a GTPase-activating protein for ARF1. EMBO J. *16*, 7305–7316.

Aoe, T., Lee, A.J., van Donselaar, E., Peters, P.J., and Hsu, V.W. (1998). Modulation of intracellular transport by transported proteins: insight from regulation of COPI-mediated transport. Proc. Natl. Acad. Sci. USA *95*, 1624–1629.

Appenzeller, C., Andersson, H., Kappeler, F., and Hauri, H.P. (1999). The lectin ERGIC-53 is a cargo transport receptor for glycoproteins. Nat. Cell Biol. *1*, 330–334.

Blum, R., Pfeiffer, F., Feick, P., Nastainczyk, W., Kohler, B., Schafer, K.H., and Schulz, I. (1999). Intracellular localization and in vivo trafficking of p24A and p23. J. Cell Sci. *112*, 537–548.

Bremser, M., Nickel, W., Schweikert, M., Ravazzola, M., Amherdt, M., Hughes, C.A., Sollner, T.H., Rothman, J.E., and Wieland, F.T. (1999). Coupling of coat assembly and vesicle budding to packaging of putative cargo receptors. Cell *96*, 495–506.

Campbell, J.L., and Schekman, R. (1997). Selective packaging of cargo molecules into endoplasmic reticulum-derived COPII vesicles. Proc. Natl. Acad. Sci. USA *94*, 837–842.

Cole, N.B., Smith, C.L., Sciaky, N., Terasaki, M., Edidin, M., and Lippincott-Schwartz, J. (1996). Diffusional mobility of Golgi proteins in membranes of living cells. Science *273*, 797–801.

Cormack, B.P., Valdivia, R.H., and Falkow, S. (1996). FACS-optimized mutants of the green fluorescent protein (GFP). Gene *173*, 33–38.

Dominguez, M., Dejgaard, K., Fullekrug, J., Dahan, S., Fazel, A., Paccaud, J.P., Thomas, D.Y., Bergeron, J.J., and Nilsson, T. (1998). gp25L/emp24/p24 protein family members of the cis-Golgi network bind both COP I and II coatomer. J. Cell Biol. *140*, 751–765.

Donaldson, J.G., Lippincott-Schwartz, J., and Klausner, R.D. (1991). Guanine nucleotides modulate the effects of brefeldin A in semipermeable cells: regulation of the association of a 110-kD peripheral membrane protein with the Golgi apparatus. J. Cell Biol. *112*, 579–588.

Ellenberg, J., E.D. Siggia, J.E. Moreira, C.L. Smith, J.F. Presley, H.J. Worman, and J. Lippincott-Schwartz. (1997). Nuclear membrane dynamics and reassembly in living cells: targeting of an inner nuclear membrane protein in interphase and mitosis. J. Cell Biol. *138*, 1193–1206.

Evan, G.I., Lewis, G.K., Ramsay, G., and Bishop, J.M. (1985). Isolation of monoclonal antibodies specific for human c-myc proto-oncogene product. Mol. Cell. Biol. *5*, 3610–3616.

Fiedler, K., Parton, R.G., Kellner, R., Etzold, T., and Simons, K. (1994). VIP36, a novel component of glycolipid rafts and exocytic carrier vesicles in epithelial cells. EMBO J. *13*, 1729–1740.

Fiedler, K., and Rothman, J.E. (1997). Sorting determinants in the transmembrane domain of p24 proteins. J. Biol. Chem. *272*, 24739–24742.

Fiedler, K., and Simons, K. (1994). A putative novel class of animal lectins in the secretory pathway homologous to leguminous lectins. Cell *77*, 625–626.

Fiedler, K., and Simons, K. (1995). The role of N-glycans in the secretory pathway. Cell *81*, 309–312.

Fiedler, K., and Simons, K. (1996). Characterization of VIP36, an animal lectin homologous to leguminous lectins. J. Cell Sci. *109*, 271–276.

Fiedler, K., Veit, M., Stamnes, M.A., and Rothman, J.E. (1996). Bimodal interaction of coatomer with the p24 family of putative cargo receptors. Science *273*, 1396–1399.

Füllekrug, J., Scheiffele, P., and Simons, K. (1999a). VIP36 localization to the early secretory pathway. J. Cell Sci. *112*, 2813–2821.

Füllekrug, J., Suganuma, T., Tang, B.L., Hong, W., Storrie, B., and Nilsson, T. (1999b). Localization and recycling of gp27 (hp24γ3): complex formation with other p24 family members. Mol. Biol. Cell *10*, 1939–1955.

Gallione, C.J., and Rose, J.K. (1985). A single amino acid substitution in a hydrophobic domain causes temperature-sensitive cell-surface transport of a mutant viral glycoprotein. J. Virol. *54*, 374–382.

Gommel, D., Orci, L., Emig, E.M., Hannah, M.J., Ravazzola, M., Nickel, W., Helms, J.B., Wieland, F.T., and Sohn, K. (1999). p24 and p23, the major transmembrane proteins of COPI-coated transport vesicles, form hetero-oligomeric complexes and cycle between the organelles of the early secretory pathway. FEBS Lett. *447*, 179–185.

Gut, A., Kappeler, F., Hyka, N., Balda, M.S., Hauri, H.P., and Matter, K. (1998). Carbohydrate-mediated Golgi to cell surface transport and apical targeting of membrane proteins. EMBO J. *17*, 1919–1929.

Hara-Kuge, S., Ohkura, T., Seko, A., and Yamashita, K. (1999). Vesicular-integral membrane protein, VIP36, recognizes high-mannose type glycans containing $\alpha 1 \rightarrow 2$ mannosyl residues in MDCK cells. Glycobiology *9*, 833–839.

Hauri, H.P., Kappeler, F., Andersson, H., and Appenzeller, C. (2000). ERGIC-53 and traffic in the secretory pathway. J. Cell Sci. *113*, 587–596.

Heim, R., Cubitt, A.B., and Tsien, R.Y. (1995). Improved green fluorescence. Nature *373*, 663–664.

Heim, R., Prasher, D.C., and Tsien, R.Y. (1994). Wavelength mutations and posttranslational autoxidation of green fluorescent protein. Proc. Natl. Acad. Sci. USA *91*, 12501–12504.

Heim, R., and Tsien, R.Y. (1996). Engineering green fluorescent protein for improved brightness, longer wavelengths and fluorescence resonance energy transfer. Curr. Biol. *6*, 178–182.

Helms, J.B. (1995). Role of heterotrimeric GTP binding proteins in vesicular protein transport: indications for both classical and alternative G protein cycles. FEBS Lett. *369*, 84–88.

Helms, J.B., Helms-Brons, D., Brugger, B., Gkantiragas, I., Eberle, H., Nickel, W., Nurnberg, B., Gerdes, H.H., and Wieland, F.T. (1998). A putative heterotrimeric G protein inhibits the fusion of COPI-coated vesicles. Segregation of heterotrimeric G proteins from COPI-coated vesicles. J. Biol. Chem. *273*, 15203–15208.

Hirschberg, K., Miller, C.M., Ellenberg, J., Presley, J.F., Siggia, E.D., Phair, R.D., and Lippincott-Schwartz, J. (1998). Kinetic analysis of secretory protein traffic and characterization of Golgi to plasma membrane transport intermediates in living cells. J. Cell Biol. *143*, 1485–1503.

Hsu, V.W., Shah, N., and Klausner, R.D. (1992). A brefeldin A-like phenotype is induced by the overexpression of a human ERD-2-like protein, ELP-1. Cell *69*, 625–635.

Itin, C., Roche, A.C., Monsigny, M., and Hauri, H.P. (1996). ERGIC-53 is a functional mannose-selective and calcium-dependent human homologue of leguminous lectins. Mol. Biol. Cell *7*, 483–493.

Itin, C., Schindler, R., and Hauri, H.P. (1995). Targeting of protein ERGIC-53 to the ER/ERGIC/cis-Golgi recycling pathway. J. Cell Biol. *131*, 57–67.

Jackson, M.E., Simpson, J.C., Girod, A., Pepperkok, R., Roberts, L.M., and Lord, J.M. (1999). The KDEL retrieval system is exploited by *Pseudomonas* exotoxin A, but not by Shiga-like toxin-1, during retrograde transport from the Golgi complex to the endoplasmic reticulum. J. Cell Sci. *112*, 467–475.

Jackson, M.R., Nilsson, T., and Peterson, P.A. (1990). Identification of a consensus motif for retention of transmembrane proteins in the endoplasmic reticulum. EMBO J. *9*, 3153–3162.

Jacquez, J.A. (1972). Compartmental analysis in biology and medicine, Amsterdam: Elsevier.

Kappeler, F., Klopfenstein, D.R., Foguet, M., Paccaud, J.P., and Hauri, H.P. (1997). The recycling of ERGIC-53 in the early secretory pathway. ERGIC-53 carries a cytosolic endoplasmic reticulum-exit determinant interacting with COPII. J. Biol. Chem. *272*, 31801–31808.

Keller, P., Toomre, D., D'az, E., White, J., and Simons, K. (2000). Multicolour imaging of post-Golgi sorting and trafficking in live cells. Nat. Cell Biol., *3*, 140–149.

Lahtinen, U., Dahllof, B., and Saraste, J. (1992). Characterization of a 58 kDa cis-Golgi protein in pancreatic exocrine cells. J. Cell Sci. *103*, 321–333.

Lewis, M.J., and Pelham, H.R. (1992). Ligand-induced redistribution of a human KDEL receptor from the Golgi complex to the endoplasmic reticulum. Cell *68*, 353–364.

Lewis, M.J., Sweet, D.J., and Pelham, H.R. (1990). The ERD2 gene determines the specificity of the luminal ER protein retention system. Cell *61*, 1359–1363.

Lippincott-Schwartz, J., Donaldson, J.G., Schweizer, A., Berger, E.G., Hauri, H.P., Yuan, L.C., and Klausner, R.D. (1990). Microtubule-dependent retrograde transport of proteins into the ER in the presence of brefeldin A suggests an ER recycling pathway. Cell *60*, 821–836.

Majoul, I., Sohn, K., Wieland, F.T., Pepperkok, R., Pizza, M., Hillemann, J., and Soling, H.D. (1998). KDEL receptor (Erd2p)-mediated retrograde transport of the cholera toxin A subunit from the Golgi involves COPI, p23, and the COOH terminus of Erd2p. J. Cell Biol. *143*, 601–612.

Melancon, P., Glick, B.S., Malhotra, V., Weidman, P.J., Serafini, T., Gleason, M.L., Orci, L., and Rothman, J.E. (1987). Involvement of GTP-binding "G" proteins in transport through the Golgi stack. Cell *51*, 1053–1062.

Moussalli, M., Pipe, S.W., Hauri, H.P., Nichols, W.C., Ginsburg, D., and Kaufman, R.J. (1999). Mannose-dependent endoplasmic reticulum (ER)-Golgi intermediate compartment-53-mediated ER to Golgi trafficking of coagulation factors V and VIII. J. Biol. Chem. *274*, 32539–32542.

Muniz, M., Nuoffer, C., Hauri, H.P., and Riezman, H. (2000). The Emp24 complex recruits a specific cargo molecule into endoplasmic reticulum-derived vesicles. J. Cell Biol. *148*, 925–930.

Nichols, W.C., Seligsohn, U., Zivelin, A., Terry, V.H., Hertel, C.E., Wheatley, M.A., Moussalli, M.J., Hauri, H.P., Ciavarella, N., Kaufman, R.J., and Ginsburg, D. (1998). Mutations in the ER-Golgi intermediate compartment protein ERGIC-53 cause combined deficiency of coagulation factors V and VIII. Cell *93*, 61–70.

Nickel, W., Sohn, K., Bunning, C., and Wieland, F.T. (1997). p23, a major COPI-vesicle membrane protein, constitutively cycles through the early secretory pathway. Proc. Natl. Acad. Sci. USA *94*, 11393–11398.

Ormo, M., Cubitt, A.B., Kallio, K., Gross, L.A., Tsien, R.Y., and Remington, S.J. (1996). Crystal structure of the Aequorea victoria green fluorescent protein. Science *273*, 1392–1395.

Pääbo, S., Weber, F., Nilsson, T., Schaffner, W., and Peterson, P.A. (1986). Structural and functional dissection of an MHC class I antigen-binding adenovirus glycoprotein. EMBO J. *5*, 1921–1927.

Pelham, H.R. (1991). Recycling of proteins between the endoplasmic reticulum and Golgi complex. Curr. Opin. Cell Biol. *3*, 585–591.

Presley, J.F., Cole, N.B., Schroer, T.A., Hirschberg, K., Zaal, K.J., and Lippincott-Schwartz, J. (1997). ER-to-Golgi transport visualized in living cells. Nature *389*, 81–85.

Robinson, M.S., and Kreis, T.E. (1992). Recruitment of coat proteins onto Golgi membranes in intact and permeabilized cells: effects of brefeldin A and G protein activators. Cell *69*, 129–138.

Rolls, M.M., Stein, P.A., Taylor, S.S., Ha, E., McKeon, F., and Rapoport, T.A. (1999). A visual screen of a GFP-fusion library identifies a new type of nuclear envelope membrane protein. J. Cell Biol. *146*, 29–44.

Saraste, J., and Svensson, K. (1991). Distribution of the intermediate elements operating in ER to Golgi transport. J. Cell Sci. *100*, 415–430.

Scales, S.J., Pepperkok, R., and Kreis, T.E. (1997). Visualization of ER-to-Golgi transport in living cells reveals a sequential mode of action for COPII and COPI. Cell *90*, 1137–1148.

Scheiffele, P., Peranen, J., and Simons, K. (1995). N-glycans as apical sorting signals in epithelial cells. Nature *378*, 96–98.

Schindler, R., Itin, C., Zerial, M., Lottspeich, F., and Hauri, H.P. (1993). ERGIC-53, a membrane protein of the ER-Golgi intermediate compartment, carries an ER retention motif. Eur. J. Cell Biol. *61*, 1–9.

Schweizer, A., Fransen, J.A., Matter, K., Kreis, T.E., Ginsel, L., and Hauri, H.P. (1990). Identification of an intermediate compartment involved in protein transport from endoplasmic reticulum to Golgi apparatus. Eur. J. Cell Biol. *53*, 185–196.

Sciaky, N., Presley, J., Smith, C., Zaal, K.J., Cole, N., Moreira, J.E., Terasaki, M., Siggia, E., and Lippincott-Schwartz, J. (1997). Golgi tubule traffic and the effects of brefeldin A visualized in living cells. J. Cell Biol. *139*, 1137–1155.

Semenza, J.C., Hardwick, K.G., Dean, N., and Pelham, H.R. (1990). ERD2, a yeast gene required for the receptor-mediated retrieval of luminal ER proteins from the secretory pathway. Cell *61*, 1349–1357.

Siemering, K.R., Golbik, R., Sever, R., and Haseloff, J. (1996). Mutations that suppress the thermosensitivity of green fluorescent protein. Curr. Biol. *6*, 1653–1663.

Sohn, K., Orci, L., Ravazzola, M., Amherdt, M., Bremser, M., Lottspeich, F., Fiedler, K., Helms, J.B., and Wieland, F.T. (1996). A major transmembrane protein of Golgi-derived COPI-coated vesicles involved in coatomer binding. J. Cell Biol. *135*, 1239–1248.

Stamnes, M.A., Craighead, M.W., Hoe, M.H., Lampen, N., Geromanos, S., Tempst, P., and Rothman, J.E. (1995). An integral membrane component of coatomer-coated transport vesicles defines a family of

proteins involved in budding. Proc. Natl. Acad. Sci. USA *92*, 8011–8015.

Storrie, B., White, J., Rötger, S., Stelzer, E.H.K., Suganuma, T., and Nilsson, T. (1998). Recycling of Golgi resident glycosyltransferases through the ER reveals a novel pathway and provides an explanation for nocodazole-induced Golgi scattering. J. Cell Biol. *143*, 1505–1521.

Tang, B.L., Low, S.H., Hauri, H.P., and Hong, W. (1995). Segregation of ERGIC53 and the mammalian KDEL receptor upon exit from the 15 degrees C compartment. Eur. J. Cell Biol. *68*, 398–410.

Tisdale, E.J., Plutner, H., Matteson, J., and Balch, W.E. (1997). p53/58 binds COPI and is required for selective transport through the early secretory pathway. J. Cell Biol. *137*, 581–593.

Toomre, D., Keller, P., White, J., Olivo, J.-C., and Simons, K. (1999). Dual-color visualization of *trans*-Golgi network to plasma membrane traffic along microtubules in living cells. J. Cell Sci. *112*, 21–33.

Townsley, F.M., Wilson, D.W., and Pelham, H.R. (1993). Mutational analysis of the human KDEL receptor: distinct structural requirements for Golgi retention, ligand binding and retrograde transport. EMBO J. *12*, 2821–2829.

Tsien, R., and Waggoner, A. (1995). Fluorophores for confocal microscopy. In: Handbook of Confocal Fluorescence Microscopy, ed. J. Pawley, New York: Plenum Press, 267–277.

Vollenweider, F., Kappeler, F., Itin, C., and Hauri, H.P. (1998). Mistargeting of the lectin ERGIC-53 to the endoplasmic reticulum of HeLa cells impairs the secretion of a lysosomal enzyme. J. Cell Biol. *142*, 377–389.

Wandinger-Ness, A., Bennett, M.K., Antony, C., and Simons, K. (1990). Distinct transport vesicles mediate the delivery of plasma membrane proteins to the apical and basolateral domains of MDCK cells. J. Cell Biol. *111*, 987–1000.

White, J., Johannes, L., Mallard, F., Girod, A., Grill, S., Reinsch, S., Keller, P., Tzschaschel, B., Echard, A., Goud, B., and Stelzer, E.H. (1999). Rab6 coordinates a novel Golgi to ER retrograde transport pathway in live cells. J. Cell Biol. *147*, 743–760.

White, J., and Stelzer, E.H.K. (1999). Photobleaching GFP reveals protein dynamics inside live cells. Trends Cell Biol. *9*, 61–65.

Yang, T.T., Cheng, L., and Kain, S.R. (1996). Optimized codon usage and chromophore mutations provide enhanced sensitivity with the green fluorescent protein. Nucleic Acids Res. *24*, 4592–4593.

Zaal, K.J., Smith, C.L., Polishchuk, R.S., Altan, N., Cole, N.B., Ellenberg, J., Hirschberg, K., Presley, J.F., Roberts, T.H., Siggia, E., Phair, R.D., and Lippincott-Schwartz, J. (1999). Golgi membranes are absorbed into and reemerge from the ER during mitosis. Cell *99*, 589–601.